Isoform-specific roles of the *Drosophila* filamin-type protein Jitterbug (Jbug) during development

SeYeon Chung[1,*], Thao Phuong Le[1], Vishakha Vishwakarma[1], Yim Ling Cheng[2] and Deborah J. Andrew[2]

[1] Department of Biological Sciences, Louisiana State University, Baton Rouge, LA 70803, USA

[2] Department of Cell Biology, Johns Hopkins University School of Medicine, Baltimore, MD 21205, USA

[*]Author for correspondence: seyeonchung@lsu.edu

Key workds: *Drosophila*, filamin, *jitterbug*, actin, thoracic bristles, epidermal denticles, tubular epithelial organs, trans-splicing

ABSTRACT

Filamins are highly conserved actin-crosslinking proteins that regulate organization of the actin cytoskeleton. As key components of versatile signaling scaffolding complexes, filamins are implicated in developmental anomalies and cancer. Multiple isoforms of filamins exist, raising the possibility of distinct functions of each isoform during development and in diseases. Here, we provide an initial characterization of *jitterbug* (*jbug*), which encodes one of the two filamin-type genes in *Drosophila*. We generate Jbug antiserum that recognizes all of the spliced forms, which reveals differential expression of different Jbug isoforms during development with a significant maternal contribution of Jbug protein. To reveal the function of Jbug isoforms, we create new genetic tools, including a null allele that deletes all isoforms, hypomorphic alleles that affect only a subset, and UAS lines for expression of the major isoforms. Using these tools, we demonstrate that Jbug is required for viability and that specific isoforms of Jbug are required in the formation of actin-rich protrusions such as thoracic bristles in adults and ventral denticles in the embryo. We also provide evidence for trans-splicing in the *jbug* locus.

Introduction

Actin-crosslinking proteins organize actin filaments into higher-order structures such as orthogonal actin arrays and parallel actin bundles. Filamins are highly conserved large cytoplasmic proteins that crosslink actin filaments into dynamic three-dimensional structures (Nakamura *et al.* 2011; Razinia *et al.* 2012). Filamins consist of actin-binding Calponin-homology (CH) domains at their N-terminus, followed by a long C-terminal rod-like domain of filamin-type immunoglobulin (IG-FLMN) repeats. Dimerization of filamins through the last C-terminal IG-FLMN repeat allows the formation of a flexible V-shaped structure that holds two actin filaments at large angles to create either a loose three-dimensional actin network (Nakamura *et al.* 2011; Razinia *et al.* 2012) or parallel bundles of actin filaments (Sokol and Cooley 1999; Gay *et al.* 2011). In addition to binding to actin, filamins interact with transmembrane receptors, adhesion molecules and even transcription factors, and are thus involved in multiple cell functions including motility, maintenance of cell shape, and differentiation (Nakamura *et al.* 2011; Razinia *et al.* 2012). Mutations in filamins are associated with a wide range of congenital anomalies and have been shown to both promote and inhibit metastasis and cancer growth (Razinia *et al.* 2012; Savoy and Ghosh 2013; Shao *et al.* 2016; Sasaki *et al.* 2019), emphasizing the multiple critical roles of filamins in development and disease.

Studies in *Drosophila* have helped refine our understanding of the roles of filamins in vivo. *Drosophila* has two orthologs of human filamin A: Cheerio (Cher) and Jitterbug (Jbug). Cher shares the organization of the protein and 46% identity and 61% similarity in amino acid sequence with human filamin A. Jbug, with 23% identity and 36% similarity in amino acid sequence with human filamin A, has some distinct features, including an actin-binding domain consisting of three, instead of two, CH domains. Several studies have revealed roles for Cher in organizing the F-actin cytoskeleton in multiple developmental contexts and diseases, including formation of ovarian germline ring canals (Li *et al.* 1999; Sokol and Cooley 1999; Huelsmann *et al.* 2016), follicle cell migration (Sokol and Cooley 2003), tissue morphogenesis during cellularization (Krueger *et al.* 2019), and *Drosophila* tumorigenesis (Külshammer and Uhlirova 2013). Compared to the extensive studies on Cher, our understanding of the roles of Jbug is more limited. Originally identified as a gene that causes bang-sensitive seizure – the phenotype that gives the gene its *jitterbug* name (Song and Tanouye 2006), *jbug* has been shown to be required in photoreceptor cells for axon targeting (Oliva *et al.* 2015) and in tendon cells to maintain their shape at the muscle-tendon junction (Olguín *et al.* 2011; Manieu *et al.* 2018).

71 Multiple isoforms of filamin proteins exist in both *Drosophila* and mammals (Sokol and Cooley
72 1999; Browne *et al.* 2000; Van der Flier and Sonnenberg 2001; Gorlin *et al.* 1990; Wang *et al.*
73 2007). Originally, only two Cher isoforms had been reported: a large isoform (FLN240) that
74 contains both actin-binding CH domains and IG-FLMN repeats and a smaller one (FLN90) that
75 contains only IG-FLMN repeats (Sokol and Cooley 1999). Recent annotations indicate that *cher*
76 encodes six longer isoforms (>240 kDa), which include two actin-binding CH domains and 18-
77 22 IG-FLMN repeats, and four shorter isoforms (90-100 kDa), which include only eight IG-FLMN
78 repeats without any CH domains (Flybase; www.flybase.org; Thurmond *et al.* 2019). Importantly,
79 a recent study in *Drosophila* larval neuromuscular junctions revealed a role for the shorter Cher
80 isoform (FLN90) in synapse formation (Lee and Schwarz 2016), suggesting distinct roles for
81 different isoforms. Like *cher*, *jbug* also encodes multiple isoforms with a range of protein sizes.
82 The roles for *jbug*, however, have been revealed mostly using RNA interference (RNAi)
83 constructs that target most of the existing splice forms, preventing the characterization of
84 isoform-specific roles for Jbug.

85 Here, we report on the creation of several new genetic tools for parsing out the roles of the
86 different Jbug isoforms, including a null allele that deletes all isoforms and hypomorphic alleles
87 that affect only a few. We also create UAS constructs for expressing some of the major Jbug
88 isoforms. We demonstrate that different isoforms are differentially expressed during
89 development and localize to different domains in embryonic epithelia. We further show an
90 essential role for Jbug in organismal viability and epithelial morphogenesis. We also show
91 isoform-specific roles of Jbug in formation of epidermal denticles during embryogenesis and
92 thoracic bristles in adults. We also report on the rescue of *jbug* function through trans-splicing.
93

Materials and Methods

Fly stocks and husbandry

Fly lines used in our experiments were: *jbug*^{20}, *jbug*^{30}, *jbug*^{133}, UAS-Jbug-RC, UAS-Jbug-RF (this work); UAS-Jbug-RL (Olguín *et al.* 2011); *Oregon R*, *fkh-Gal4* (Henderson and Andrew 2000), *69B-Gal4* (Rorth 1996); *da-Gal4* (Wodarz *et al.* 1995); *mat*α*-Gal4* (Häcker and Perrimon 1998), *Df(2R)59AB*, *Df(2R)Exel6079*, *TRiP.JF01116* (Bloomington Stock Center); *GD8664*, *GD13033* (Vienna *Drosophila* RNAi Center). All crosses were performed at 25°C.

Generation of *jbug* mutant alleles

jbug mutants were generated by homologous recombination (Gong and Golic 2003). For *jbug*^{20} null mutants, genomic fragments upstream and downstream of the *jbug* ORF were amplified by PCR using the following primers (restriction sites in bold and linkers in italic):

in-fusion_L-22737893, 5'-*CTAGTCTAGGGCGCGCC*GATGAGTTGTGGCTTGAGCA-3'
in-fusion_R-22742442, 5'-*TAGGGGATCACGTACG*GCCAAACCAATGCTGAAGAT-3'
NotI_L-22717574, 5'-AT**GCGGCCGC**TAGAGGGGAGAGCAAGTGGA-3'
Acc65I_R-22721186, 5'-ATA**GGTACC**GTGTGAGCTTCGGGATCAAT-3'

For *jbug*^{30} and *jbug*^{133} hypomorphic alleles, genomic fragments upstream and downstream of an exon common to all *jbug* splice forms were amplified using the following primers (restriction sites in bold):

AscI_L-22727168, 5'-AT**GGCGCGCC**AAAGCCGTTGAAGAAAGCAA-3'
BsiWI_R-22731840, 5'-ATA**CGTACG**CTCGATGCACTTTGTCTCCA-3'
NotI_L-22717574, 5'-AT**GCGGCCGC**TAGAGGGGAGAGCAAGTGGA-3'
Acc65I_R-22721186, 5'-ATA**GGTACC**GTGTGAGCTTCGGGATCAAT-3'

PCR fragments were cloned into pW25, which carries *white*$^{+}$, the recognition site for I-SceI endonuclease, and FRT sites. The constructs were injected into *w*^{1118} embryos by Rainbow Transgenic Flies, Inc. Transformants were crossed to flies carrying hs-I-SceI and hs-Flp and progeny were heat shocked (37°C) for 1 hour 48–72 hours after egg laying (AEL). Recombination and insertion were confirmed by genomic PCR and reverse-transcriptase PCR (RT-PCR) followed by sequencing.

124 The following primers were used for RT-PCR for *jbug*[20] shown in Supplemental Figure 1
125 (restriction sites in bold and linkers in italic):

126 *jbug* 5-1, 5'-GGAGAACAAGTACCGGGTGA-3'
127 *jbug* 5-2, 5'-*GGATCCTCGAGCATATG*TCCTTCCACGTTCACCTCGA-3' (same as Jbug-Ab-3'
128 for making Jbug antibody)
129 *jbug* 3-1, 5'-AT**GCGGCCGC**TAGAGGGGAGAGCAAGTGGA-3' (same as NotI_L-22717574
130 used for amplifying a homology arm downstream of the *jbug* ORF)
131 *jbug* 3-2, 5'-*CGCGCGGCAGCCATATG*ATGTCCTCACCCGGCCTAAC-3' (same as Jbug-Ab-5'
132 for making Jbug antibody)
133

134 **Generation of UAS-Jbug-RC and -RF transgenic flies**

135 An ORF for *jbug-RC* (1230 bp) was PCR-amplified using the existing cDNA RE40504 as a
136 template. A full cDNA for *jbug-RF* (9430 bp) was created by In-Fusion cloning of three
137 fragments. The 5' fragment was prepared by enzyme digestion of RE40504 (cut with ApaI and
138 BamHI). The middle fragment (1189 bp) was amplified by reverse transcriptase-PCR (RT-PCR)
139 and the ApaI and BglII sites were added to the 5' and the 3' end of the fragment, respectively.
140 The 3' fragment was amplified by PCR using GH03118 from the BglII site to the end of the ORF
141 and the BamHI site was added to the 3' end. The ligated full cDNA was confirmed by
142 sequencing. *jbug-RC* and *jbug-RF* ORFs were PCR-amplified and cloned into the pUAST vector
143 (Brand and Perrimon, 1993) to create UAS-Jbug-RC and UAS-Jbug-RF. The DNA constructs
144 were injected into *w*[1118] embryos by Rainbow Transgenics, Inc. (UAS-Jbug-RC) and by
145 GenetiVision (UAS-Jbug-RF).
146

147 **Generation of Jbug antibody**

148 A PCR fragment of 1212 bp that is common to all *jbug* splice forms was cloned into the pET15b
149 vector. The fragment corresponds to almost the entire open reading frame for the Jbug-PC
150 isoform except for the last six amino acids and contains four IG-FLMN repeats. Primers used for
151 In-Fusion cloning were (restriction sites in bold and linkers in italic):

152 Jbug-Ab-5', 5'- *CGCGCGGCAGCCATATG*ATGTCCTCACCCGGCCTAAC-3'
153 Jbug-Ab-3', 5'- *GGATCCTCGAGCATATG*TCCTTCCACGTTCACCTCGA-3'

154 The construct was transformed into BL21-DE3 cells for protein induction with IPTG.
155 Recombinant protein was purified using Ni-NTA agarose (Qiagen). Rabbit polyclonal antibodies

156 were generated by Covance, Inc. and used at a dilution of 1:500 for immunohistochemistry and
157 1:5,000 for western blot.
158
159 **Western blot**
160 Protein extracts from embryos 0-2 and 2-16 hours AEL, 1st, 2nd, 3rd instar larvae, pupae (2 days
161 after puparium formation (APF), and 2-day old male and female adults were used. For embryos
162 homozygous for *jbug*^{20}, *Df(2R)59AB* and *Df(2R)Exel6079* and for 1st instar larvae homozygous
163 for *jbug*^{20} and transheterozygous for *jbug*^{30}/*Df(2R)Exel6079*, a balancer chromosome that
164 contains the twi-Gal4 UAS-GFP construct was used to distinguish desired genotypes from
165 heterozygous siblings. Rabbit α-Jbug (this work; 1:5,000), mouse α-Actin (RRID:AB_11004139;
166 Invitrogen; 1:2,000), and HRP-labelled secondary antibodies (RRID:AB_430833;
167 RRID:AB_430834; Promega; 1:2,000) were used. Protein bands were detected using Pierce
168 ECL Western Blotting Substrate.
169
170 **Scanning electron microscopy**
171 Wild type (*Oregon R*) and *jbug*^{30} homozygous male flies were coated with gold palladium and
172 examined and photographed in a LEO/Zeiss Field-emission SEM.
173
174 **Antibody staining and confocal microscopy**
175 Embryos were collected on grape juice-agar plates and processed for immunofluorescence
176 using standard procedures. Briefly, embryos were dechorionated in 50% bleach, fixed in 1:1
177 heptane:formaldehyde for 40 min and devitellinized with 80% EtOH, then stained with primary
178 and secondary antibodies in PBSTB (1X PBS, 0.1% Triton X-100, 0.2% BSA). For Jbug and
179 phalloidin staining, embryos were hand-devitellinized. Antibodies used include: mouse α-Crb
180 (RRID: AB_528181; DSHB 1:10), rabbit α-CrebA (RRID: AB_10805295; 1:5,000), guinea pig α-
181 Sage (Fox *et al.* 2013) , chicken α-GFP (RRID:AB_2534023; Invitrogen; 1:500), rat α-E-Cad
182 (RRID: AB_528120; DSHB; 1:50), rabbit α-Jbug (this work; 1:500), rabbit α-β-Gal (RRID:
183 AB_221539; Invitrogen; 1:500). Alexa fluor 488, 568, 647-labelled secondary antibodies were
184 used at 1:500 (RRID: AB_142924; RRID: AB_141778; RRID: AB_2535766; RRID: AB_143157;
185 RRID: AB_2535812; Molecular Probes). Alexa fluor-568-labeled phalloidin was used for F-actin
186 labelling (RRID: AB_2632953; Molecular Probes; 1:250). All images were taken with a Leica
187 SP8 confocal microscope using either a 63x, 1.4 NA or a 40x, 1.3 NA oil objective and the LAS
188 X software (Leica).
189

190 **Quantification of denticle precursors in the ventral epidermis**

191 Embryos stained for phalloidin and E-Cad were imaged with a Leica SP8 confocal microscope.
192 A maximum intensity projection was generated using two focal planes (0.3 μm apart) in the
193 region of adherens junctions. Denticle belts in abdominal segments 4-6 in stage 16 embryos
194 were selected for quantification. Six columns of cells from anterior to posterior of each belt were
195 analyzed. In each column, denticle precursors of four cells closest to the ventral midline were
196 counted. For each genotype, five to eight embryos were quantified. Unpaired Student's t-test
197 with Welch's correction was used for statistical analysis.

198

199 **Results**

200 **Different splice forms of *jbug* are differentially expressed during development**

201 Ten annotated splice forms of *jbug*, which encode six different protein isoforms, are reported in
202 Flybase (www.flybase.org; Thurmond *et al.* 2019). All isoforms contain multiple repeats of
203 filamin-type immunoglobulin (IG-FMLN) domains (Figure 1, A and B), which form a rod-like
204 structure in filamin. Two Jbug isoforms consist exclusively of these repeats; Jbug-PC/G/H/J/K
205 (each splice form encodes the same 42.4 kDa protein; hereafter refered to as Jbug-PC) has four
206 IG-FMLN repeats and Jbug-PI (185.7 kDa) has sixteen (Figure 1B). On the other hand, Jbug-PL
207 (175.6 kDa) and Jbug-PF/M/N, the three longest Jbug isoforms (>300 kDa), contain three
208 tandem calponin-homology (CH) actin-binding domains in their N-termini as well as multiple IG-
209 FMNLs in their C-termini (seven and nineteen IG-FMLNs for Jbug-PL and Jbug-PF/M/N,
210 respectively) (Figure 1B).

211 High-throughput expression data available in Flybase (www.flybase.org; Thurmond *et al.* 2019)
212 showed high expression of *jbug* splice forms throughout all developmental stages, except during
213 0-18 hour embryogenesis when there is very little expression of *jbug-RF, RM, RN* and *jbug-RL*
214 (Figure 1C; FB2020_04). To analyze protein expression levels of Jbug during *Drosophila*
215 development, we generated Jbug antiserum that recognizes a protein domain encoded by all
216 ten *jbug* splice forms (Figure 1A). This domain includes the four IG-FLMN repeats that are
217 present in all Jbug isoforms (Figure 1B). Our Western blot analysis using wild-type protein
218 extracts revealed that Jbug proteins are detected at high levels throughout all developmental
219 stages (Figure 1D). Strong Jbug signals in protein extracts from 0-2 hour embryos (Figure 1D)
220 also suggest a maternally provided pool of Jbug.

221 The Jbug antiserum detected bands in the size ranges that are predicted from the major splice
222 forms (42.4 kDa, 175.6 kDa, 185.7 kDa, >300 kDa). Importantly, the different isoforms were
223 differentially expressed during development (Figure 1D). Jbug-PC (42.4 KDa) was abundant
224 only in pupae and Jbug-PL (175.6 kDa) was most abundant in adults (Figure 1D). Bands
225 corresponding in size to Jbug-PI (185.7 kDa) and Jbug-PF/M/N (>300 kDa) were detected at all
226 stages with slight differences in protein levels (Figure 1D). Jbug-PF/M/N isoforms differ only
227 slightly from one another in regions outside the CH and IG-FLMN domains. Due to their huge
228 sizes and a very slight difference in molecular weight among Jbug-PF/M/N, we were not able to
229 distinguish exactly which of the three isoforms is expressed at any specific stage. The large size
230 of these isoforms also diminishes membrane transfer, leading to relatively weak signals. Notably,
231 several intermediate-sized bands that did not match the predicted size of annotated isoforms

232 were also detected at different levels throughout development (Figure 1D). The existence of
233 these bands suggests either that more Jbug isoforms exist than have been annotated or that
234 proteolyzed and/or phosphorylated fragments are being detected (also see Figure 2F; most of
235 these extra bands are absent in *jbug* null mutant larval extracts). Indeed, roles for proteolytic
236 forms of Filamin A (Bedolla *et al.* 2009; Savoy and Ghosh 2013; Yue *et al.* 2013) as well as
237 phosphorylated Filamin A (Ohta and Hartwig 1996; Tirupula *et al.* 2015) have been reported
238 from studies of the mammalian proteins. Taken together, our data indicate that different splice
239 forms of *jbug* are differentially expressed during *Drosophila* development.
240

241 **Null and hypomorphic *jbug* alleles have been generated**

242 To investigate roles for *jbug* in development, we generated mutant alleles for *jbug* using
243 homologous recombination (Gong and Golic 2003). Two donor DNA constructs were used to
244 target different genomic regions. One construct targets the genomic region encompassing the
245 translation start sites for all splice forms and extends through the exons shared by all splice
246 forms; the other targets only the region containing the exons shared by all splice forms (Figure 2,
247 A and B). With the construct that targets the larger region, we obtained a null mutant, $jbug^{20}$
248 (Figure 2A). PCR analysis confirmed that the entire targeted region was replaced with the mini-
249 $white^{+}$ (mini-w^{+}) gene (data not shown). Reverse transcriptase-PCR (RT-PCR) using mRNA
250 extracted from homozygous $jbug^{20}$ embryos further confirmed that no *jbug* transcripts are
251 produced in $jbug^{20}$ embryos (Supplemental Figure 1, A-C). Both $jbug^{20}$ homozygous animals
252 and transheterozygotes for $jbug^{20}$ over either of the two deficiency lines that delete all or part of
253 the *jbug* locus (*59AB* and *Exel6079*; Figure 2A) died during the first instar larval stage (Table 1).
254 Western blot analysis using Jbug antiserum showed that whereas a significant amount of the
255 Jbug proteins were detected in $jbug^{20}$ embryos (Figure 2E), almost all protein bands were
256 absent by the first instar larval stage, with the exception of two low molecular weight bands that
257 are likely to be from nonspecific cross-reactivity (Figure 2F). Similarly, all Jbug isoforms were
258 detected both in *59AB* and *Exel6079* homozygous embryos (Figure 2I). These data suggest that
259 Jbug proteins from maternally provided *jbug* mRNA or protein persist through embryogenesis.
260 Since only very low level of *jbug* mRNA is detected in 0-2 hour wild-type embryos, based on
261 RNA-Seq (Flybase; www.flybase.org) and in situ hybridization (Fly-FISH; http://fly-
262 fish.ccbr.utoronto.ca), it is more likely that the Jbug protein, and not the mRNA, is maternally
263 provided.

264 With the DNA construct that aimed to replace the genomic region common for all splice forms of
265 *jbug*, we unexpectedly obtained two hypomorphic alleles, *jbug*^{30} and *jbug*^{133}, that affect only a
266 subset of splice forms (Figure 2, B-D). Incomplete recombination occurred in these two alleles,
267 resulting in either a part (for *jbug*^{30}) or the entire DNA construct (for *jbug*^{133}) being inserted into
268 the *jbug* locus (Figure 2B). In *jbug*^{30}, one homology arm in the donor DNA recombined correctly,
269 but the other homology arm was inserted into the genome along with the mini-*w*+ gene, rather
270 than being recombined (Figure 2C). In *jbug*^{133}, homologous recombination failed to occur;
271 instead, the entire donor construct was inserted into the 3' UTR of the splice forms that have
272 longer C-termini (*jbug-RI* and *jbug-RF*/*M*/*N*) (Figure 2D). These recombination events disrupt
273 *jbug-RI* and *jbug-RF*/*M*/*N* in both alleles. Western blot analysis revealed that the Jbug-PF/M/N
274 isoforms (>300 kDa) were either absent or decreased to undetectable levels in *jbug*^{30} mutants at
275 all stages (Figure 2, E-H and J). Jbug-PI (185.7 kDa) was also absent in *jbug*^{30}, and instead, a
276 smaller protein (~90 kDa) was detected in *jbug*^{30} mutant animals at all stages (Figure 2, E-H and
277 J). This additional band was not detected in wild type or *jbug*^{133} protein extracts at any stages,
278 suggesting that insertion of the DNA construct generates a truncated form of Jbug-PI in *jbug*^{30}.
279 In *jbug*^{133}, both Jbug-PF/M/N and Jbug-PI protein bands were slightly decreased in intensity
280 (Figure 2, E-H), suggesting that insertion of the construct in the 3' UTR region either affects
281 mRNA stability or inhibits translation of these isoforms. Consistent with the molecular data, we
282 did not detect any significant changes in the level of Jbug-PC (42.4 kDa) and Jbug-PL (175.6
283 kDa) in *jbug*^{30} and *jbug*^{133} protein extracts (Figure 2, E-H). Taken together, we generated new
284 alleles for *jbug*, including a null mutant and two hypomorphic alleles that disrupt a subset of
285 Jbug isoforms, specifically Jbug-PI and Jbug-PF/M/N.
286
287 ***jbug* hypomorphs show semi-lethality and defects in bristle development on the thorax**
288 Many homozygous flies in *jbug*^{30} and *jbug*^{133} died during pupation, leaving a number of dead
289 pupae that never eclosed. In both alleles, homozygous adult flies that survived were fertile and
290 homozygous lines could be maintained. Interestingly, adult flies homozygous for *jbug*^{30} or
291 *jbug*^{133} produced short, bent and rough-ended bristles on the thorax (Figure 3A), suggesting a
292 role for Jbug in bristle development, perhaps in crosslinking actin bundles that form the bristles.
293 Consistent with our findings that levels of Jbug-PF/M/N and Jbug-PI were more significantly
294 reduced in *jbug*^{30} than in *jbug*^{133} (Figure 2, E-H), *jbug*^{30} flies showed a higher expressivity of
295 bristle defects than *jbug*^{133}. Whereas almost every thoracic bristle had defects in *jbug*^{30}
296 homozygous adults, only a few bristles showed distinguishable defects in *jbug*^{133} homozygotes
297 (Figure 3A).

298 To analyze the bristle defects in more detail, we performed scanning electron microscopy (SEM)
299 in wild type and *jbug*^{30} homozygous mutant adults. Whereas wild-type animals showed nicely
300 elongated and tapered bristles that suggested evenly aligned actin bundles (Figure 3B, a and a'),
301 *jbug*^{30} mutant flies had bristles that were short, curved (Figure 3B, c), bent (Figure 3B, d) and
302 rough-ended (Figure 3B, e). Even when the bristles looked relatively normal, they were often
303 shorter than wild type and mildly twisted (Figure 3B; compare b and b' to f and f').

304 Transheterozygotes of *jbug*^{30} or *jbug*^{133} over the *jbug*^{20} null allele or the *59AB* deficiency line that
305 deletes the entire *jbug* gene (Figure 2, C and D) showed both semi-lethality and the same bristle
306 defects as observed in homozygous *jbug*^{30} and *jbug*^{133} adults (Table 1). These data suggest that
307 both phenotypes are due to loss of *jbug* function. Consistent with our data that *jbug*^{30} is a more
308 severe hypomorphic allele than *jbug*^{133} (Figure 2, E-H; Figure 3A), fewer transheterozygous
309 *jbug*^{30}/*jbug*^{20} or *jbug*^{30}/*59AB* flies survived to the adult stage compared to transheterozygous
310 *jbug*^{133}/*jbug*^{20} or *jbug*^{133}/*59AB* flies (Table 1). Taken together, these data suggest that Jbug-
311 PF/M/N and/or PI are important for viability and for actin bundle arrangement within bristles.

312 We also performed complementation tests using the deficiency line *Exel6079*, which deletes
313 through the genomic region encoding the N-terminal exons of transcripts of *jbug-RL* and *jbug-*
314 *RF/M/N*, but leaves the coding region for *jbug-RC* and *jbug-RI* intact (Figure 2, C and D).
315 Interestingly, transheterozygous *jbug*^{30}/*Exel6079* (and *jbug*^{133}/*Exel6079*) flies showed neither
316 semi-lethality nor bristle defects (Table 1). This finding was unexpected because Jbug-PF/M/N
317 should be absent in transheterozygous *jbug*^{30}/*Exel6079* flies; *jbug*^{30} and *Exel6079* disrupt the 3'
318 and the 5' ends of *jbug-RF/M/N*, respectively. To test which isoforms are present in
319 *jbug*^{30}/*Exel6079* flies, we performed Western blot using extracts from *jbug*^{30}*/Exel6079*
320 transheterozygous 1st instar larvae. Surprisingly, strong Jbug-PF/M/N bands were detected in
321 *jbug*^{30}*/Exel6079* (Figure 2J). The rescue of *jbug*^{30} *and Jbug*^{133} phenotypes by *Exel6079* and the
322 presence of protein isoforms that should be missing in either *Exel6079* or in the *jbug*
323 hypomorphic alleles, suggest some form of trans-splicing, wherein the 5' exons encoded on the
324 *jbug* hypomorphic chromosomes are spliced to 3' exons encoded on the *Exel6079* chromosome.
325

326 **Expression of Jbug-RF rescues the bristle defects and semi-lethality of *jbug* hypomorphs**
327 To begin to parse out the functions of the different Jbug isoforms, we created two new UAS-
328 lines, one encoding Jbug-PC (42 kDa protein) and one encoding Jbug-PF (>300 kDa protein).
329 We also obtained a UAS construct for Jbug-PL (175.6 kDa protein) expression from the Mlodzik
330 lab (Olguín *et al.* 2011). We first tested whether expression of any specific *jbug* splice form(s)

331 could rescue the lethality of *jbug*^{20} null mutants. Each of the three constructs was expressed in
332 *jbug*^{20} mutant background using *daughterless-Gal4* (*da-Gal4; Wodarz et al., 1995*), which is
333 expressed in all cells, or *69B-Gal4* (Rorth 1996), which is expressed in ectodermal cells. None
334 of the UAS-constructs rescued the lethality of *jbug*^{20}; indeed, no larvae survived past the 1st
335 instar larval stage. These data suggest that multiple Jbug isoforms are required for viability.

336 We next tested whether expression of specific Jbug isoforms could rescue the bristle defects in
337 *jbug*^{30}, the severe hypomorphic allele. Consistent with the data that Jbug-PC is not affected in
338 *jbug*^{30} mutants, overexpression of *jbug-RC* with *da-Gal4* or with *69B-Gal4* in an otherwise wild-
339 type background did not result in any overt defects in bristles (Figure 3C) nor did it rescue the
340 bristle defects of *jbug*^{30} homozygotes (Figure 3E). On the other hand, overexpression of *jbug-*
341 *RF* in otherwise wild-type animals resulted in shorter and thicker bristles (Figure 3D), suggesting
342 that proper levels of Jbug-PF/M/N are critical for normal bristle development. Importantly,
343 expression of *jbug-RF* in *jbug*^{30} mutants using *da-Gal4* or *69B-Gal4* nearly completely rescued
344 the bristle phenotypes (Figure 3F). Moreover, *jbug-RF* expression in *jbug*^{30} mutants also
345 rescued semi-lethality. 86% (27/32) of pupae emerged as adult flies when jbug-RF was
346 overexpressed in *jbug*^{30} mutants whereas only 26% (9/35) of *jbug*^{30} homozygous pupae
347 emerged as adult flies. These data suggest that the bristle defects and semi-lethality observed
348 in *jbug*^{30} are due to loss of the longest (>300 kDa) Jbug isoforms.
349

350 **Jbug hypomorphs show delay in actin-based prehair formation and mild defects in wing**
351 **hair orientation**

352 Besides thoracic bristle defects, *jbug*^{30} and *jbug*^{133} homozygous adults also showed a mild
353 swirling pattern of wing hairs (Supplemental Figure 2, B and C). Phalloidin staining of actin-rich
354 prehairs at 32 hours after puparium formation (APF) revealed that hair formation is delayed in
355 *jbug*^{30} pupal wings (Supplemental Figure 2, D and E). A swirling pattern of wing hairs and
356 delayed prehair formation are often observed in mutants for planar cell polarity (PCP) genes
357 (Adler 2012). *jbug*^{30} mutant eyes, however, did not have any defects in ommatidial rotation
358 characteristic of loss of key PCP genes (Supplemental Figure 2, F and G), suggesting that Jbug
359 is not involved in ommatidial rotation. Overall, these data suggest that proper levels for Jbug-
360 PF/M/N and/or Jbug-PI are required for the timely maturation of the actin bundles that form the
361 prehairs.
362

363 **Jbug proteins localize in a dynamic pattern in the embryonic epithelium**

364 We next analyzed the subcellular localization of Jbug proteins during embryogenesis in wild
365 type and *jbug* mutant alleles. During early development, Jbug was detected as small punctate
366 structures in the cytoplasm of all cells (Figure 4A). During stages 11-13, Jbug was detected at a
367 high level both near the apical surface and at and near the adherens junctions (AJs) in all
368 epidermal cells (Figure 4B). AJ Jbug signals became weaker over time, and by stage 15, only
369 mesh-like signals on the apical surface remained (Figure 4C). In $jbug^{20}$ mutant embryos, AJ
370 signals were absent but strong signals on the apical surface were still detected (Figure 4D). At
371 stage 15 and later, apical surface signals were slightly decreased compared to wild type levels
372 (Figure 4E). Since the $jbug^{30}$ and $jbug^{133}$ homozygotes that survived to adult stages were fertile,
373 we analyzed Jbug signals in $jbug^{30}$ or $jbug^{133}$ embryos from homozygous mothers. Interestingly,
374 in $jbug^{30}$ embryos from $jbug^{30}$ homozygous mothers, Jbug signals were both very weak and
375 dispersed in epidermal cells throughout the stages, and largely absent in AJs (Figure 4, F and
376 G), suggesting that Jbug-PF/M/N and Jbug-PI might be major isoforms that show strong
377 embryonic expression and AJ localization. Expression of Jbug-RF in the $jbug^{30}$ mutant
378 background restored strong signals at AJs (Figure 4G) and on the apical surface (Figure 4K) at
379 stage 13 and 15, respectively. Consistent with the minor changes in Jbug protein levels in
380 $jbug^{133}$, Jbug staining was mostly normal, albeit slightly reduced, in the epidermal cells in $jbug^{133}$
381 embryos from homozygous $jbug^{133}$ mothers (Figure 4, H and I).

382 BDGP Expression Data showed that, in addition to the strong ectodermal expression at earlier
383 stages, *jbug* is also upregulated in epithelial tubular organs, including the trachea and the
384 salivary gland (https://insitu.fruitfly.org/cgi-bin/ex/insitu.pl). Our previous work also showed that
385 tracheal expression of *jbug* is upregulated by Trachealess, a major transcription factor in the
386 trachea (Chung *et al.* 2011). Consistent with mRNA expression, antibody staining in wild-type
387 embryos revealed accumulation of Jbug protein in the trachea and the salivary gland (Figure 5,
388 A and E). Interestingly, Jbug was abundant in both the cytoplasm and in a distinct apical domain
389 of both tracheal and salivary gland cells, which appeared to be just under the apical
390 surface(Figure 5, A and E), as opposed to following the AJ pattern of E-Cad. This apical staining
391 was prominent up to stage 14 in the salivary gland; at later stages, Jbug signals were observed
392 mostly in the cytoplasm and detected in the apical domain only as a thin layer along the lumen
393 (compare Figure 5E to Figure 6A).

394 Jbug signals in tubular epithelial organs were significantly decreased in $jbug^{20}$ embryos, even
395 with regards to surrounding tissues (Figure 5, B and F), suggesting that zygotic *jbug* expression
396 is required for upregulation of Jbug in these tissues. In $jbug^{20}$, the apical staining in the trachea

397 was absent and in the salivary gland was more punctate. In *jbug*^{30}, apical staining of Jbug in the
398 trachea and salivary glands was also absent; instead, uniform Jbug signals were detected in the
399 cytoplasm (Figure 5, C and G). Consistent with slight changes in Jbug protein levels in *jbug*^{133},
400 Jbug signals were mostly normal, albeit slightly reduced, in the trachea and salivary glands in
401 *jbug*^{133} (Figure 5, D and H; data not shown). These data suggest that Jbug-PF/M/N (>300 kDa)
402 and/or Jbug-PI (185 kDa) are enriched in the apical domain in tubular epithelial organs in the
403 embryo.

404 **Jbug function in embryonic epithelial tubes**

405 Despite the absence or mislocalization of Jbug in the apical domain of trachea and salivary
406 glands, both organs developed normally without showing overt morphological defects in *jbug*^{20}
407 and *jbug*^{30} embryos (Figure 5, B, C, F and G). To ask if maternally supplied *jbug* is sufficient for
408 embryonic development, we maternally knocked down *jbug* using the *mat*α*-Gal4* driver (Häcker
409 and Perrimon 1998) to *express a jbug* RNAi construct that targets all *jbug* splice forms. Maternal
410 knockdown of *jbug* did not result in overt defects in overall embryo morphology (data not shown).
411 However, knockdown of *jbug* both maternally and zygotically using *mat*α*-Gal4* and *fork head-*
412 *Gal4* drivers (*fkh-Gal4*; a driver that drives expression in several embryonic tissues including the
413 salivary gland; Henderson and Andrew 2000) resulted in severe morphological defects in the
414 embryo, including deeper segmental grooves and a wider salivary gland lumen (Figure 5J).
415 These data suggest that both maternal or zygotic pools of *jbug* are required for tubular epithelial
416 organ morphogenesis.

417 To test the effect of Jbug overexpression in tubular epithelial tissues, we overexpressed
418 different Jbug isoforms (Jbug-PC, PL and PF) in the salivary gland using *fkh*-Gal4. Interestingly,
419 overexpression of each isoform caused an expanded and irregular apical domain (Figure 6, B-
420 F). Moreover, the apical protein Crb, which is normally enriched in a sub-apical domain just
421 apical to the AJs in many epithelial cells including salivary gland cells (Fig 6A, inset in Crb
422 column; Wodarz *et al.* 1995; Tepass 1996; Chung and Andrew 2014), was mislocalized and
423 dispersed along the entire apical surface in Jbug-overexpressing salivary glands (Figure 6, B-F).
424 These data indicate that overexpression of multiple Jbug isoforms can disrupt the sub-apical
425 domain enrichment of Crb. Interestingly, unlike other isoforms that are primarily localized in the
426 cytoplasm when overexpressed (Figure 6, D-F), both untagged and C-terminal GFP-tagged
427 Jbug-PC were detected in the cytoplasm and in nuclei (Figure 6, B and C). These data suggest
428 that this smallest isoform – which is primarily expressed in pupae (Figure 1D) – might function in

429 the nucleus as well. Taken together, these data suggest that appropriate levels of Jbug isoforms
430 are important for apical organization of tubular epithelial cells during organ development.
431
432 **Jbug is required for denticle formation in the epidermis**
433 Jbug antibody staining in the ventral regions of stage 14 embryos revealed intense signals on
434 the apical surface that presaged the actin-rich denticles that begin to form during stage 15
435 (Figure 7, B and C). This prompted us to ask if denticle formation was normal in *jbug* mutants. In
436 wild type embryos, six rows of epidermal cells in the anterior portion of each segment normally
437 produce one or more denticles, forming a trapezoidal belt (Bejsovec 2013; Figure 7, C and D;
438 Figure 8A). Embryos homozygous for $jbug^{20}$ did not show any overt morphological defects, likely
439 due to strong maternal contribution (see Figure 1D and 2E), but they exhibited defects in
440 denticle formation. Similarly, $jbug^{30}$ embryos from a homozygous stock also exhibited defects in
441 denticle formation, suggesting that Jbug-PF/M/N and/or Jbug-PI are important for actin bundle
442 arrangement within denticles. Whereas the trapezoidal belts of actin-rich pre-denticles were
443 relatively normal overall, there were both fewer and smaller denticle structures in $jbug^{20}$ and
444 $jbug^{30}$ mutants compared to wild type (Figure 8, A-C). We counted the number of denticles in
445 each cell from a grid of 24 cells (Figure 8H) for at least five individuals of each genotype. $jbug^{20}$
446 embryos had fewer denticles per cell than wild type embryos in several rows of cells (C1, C3,
447 C4 and C6; Figure 8, I and J). Irrespective of which row of cells (C1-C6) was examined, $jbug^{30}$
448 embryos had, on average, fewer denticles per cell than wild type embryos (Figure 8, I and J).
449 Expression of *jbug-RF* using the *da-Gal4* driver in $jbug^{30}$ mutants slightly increased the number
450 of denticles in one row (C1), but not in other rows (C2-C6). Knocking down *jbug-RL* and *jbug-*
451 *RF/M/N* by RNAi (*GD13033*; Figure 1A) using *da-Gal4* also showed a decrease in the numbers
452 of denticles per cell in rows C4 and C6 compared to wild type (Figure 8, F, I and J).

453 To test for a role of maternally provided Jbug in embryogenesis, we knocked down *jbug* by
454 expressing each of the three RNAi lines that target different regions of *jbug* splice forms (Figure
455 1A) using a maternal driver *matα-Gal4*. Knocking down *jbug* using two strong RNAi lines
456 (*GD8664* and *GD13033*; Figure 1A) resulted in very few embryos, suggesting an essential role
457 for Jbug in oogenesis. Knocking down *jbug* using a weak RNAi line *JF01166* (Figures 1A)
458 resulted in embryos with mild morphological defects such as slightly wavy epidermis and deeper
459 grooves for some segmental grooves (Figure 8, G and L), suggesting that maternally provided
460 Jbug proteins are required for normal development. These embryos also showed defects in
461 denticle formation. As observed in $jbug^{20}$ and $jbug^{30}$ mutants or *da-Gal4>jbug RNAi* embryos,

462 some cells failed to form denticles (Figure 8, G and I); others formed short denticles with weak
463 phalloidin signals (Figure 8G). Quantification showed a decrease in the average number of
464 denticles per cell in most columns (except for C2) of each denticle belt with *matα>jbug RNAi*
465 (Figure 8J). Taken together, our data suggest that both maternally and zygotically provided
466 Jbug proteins are required for denticle formation.
467

468 **Discussion**

469 Filamins play important roles in actin reorganization in many developmental processes and
470 disease contexts. In this study we show that different isoforms of Jbug, the *Drosophila* filamin-
471 type protein, are differentially expressed during development. Using new genetic tools that we
472 generated, we reveal essential roles for different Jbug isoforms in viability, epithelial
473 morphogenesis and formation of actin-rich structures.

474

475 **Jbug plays a role in formation of actin-rich protrusions**

476 Our results identify isoform-specific roles for Jbug in formation of two prominent actin-rich
477 protrusions in *Drosophila*, bristles on the thorax and denticles in the ventral epidermis of the
478 embryo (Figures 3 and 8). These defects are observed in the presence of Jbug-PL, which
479 contains actin-binding domains and short IG-FLMN repeats, suggesting that this isoform is not
480 sufficient to form actin-rich protrusions in *Drosophila*. Indeed, bristle defects are rescued by
481 expression of Jbug-PF, one of the longest isoforms that contain long IG-FLMN repeats following
482 the actin-binding domains (Fig. 3). These data suggest an important role for protein interactions
483 through the long IG-FLMN repeats in forming actin-rich protrusions. Our interpretation is
484 consistent with a role of filamins in acting as a molecular scaffold. More than 90 filamin-binding
485 partners have been identified, including intracellular signaling molecules, receptors, ion
486 channels, transcription factors, and cytoskeletal and adhesion proteins (Razinia et al., 2012).

487 Unlike defects in thoracic bristles, defects in denticle formation, although improved, were not
488 fully rescued by overexpression of *jbug-RF* in *jbug*^{30} mutant embryos (Figure 8). These data
489 suggest that either Jbug-PI, an isoform that contains long IG-FLMN repeats without actin-
490 binding domains, might contribute to this process or that the expression system failed to provide
491 enough of the *jbug-RF* splice form for rescue. Although Jbug is upregulated in the anterior side
492 of each segment in the embryo, where denticle belts form, Jbug is not enriched in the denticles
493 themselves (Figure 7). Interestingly, another *Drosophila* filamin – Cher – is enriched in denticles,
494 colocalizing with actin protrusions (Dilks and DiNardo 2010). The different subcellular
495 localization of Jbug and Cher in denticle forming cells suggests distinct roles for the two
496 *Drosophila* filamins. Cher likely acts as a component of denticles that organizes actin filaments.
497 A simple model for Jbug function is that the N-terminal actin-binding domains might act to
498 stabilize actin filaments and that protein-protein interactions through long IG-FLMN repeats
499 might recruit other key components for denticle formation to the apical plasma membrane where
500 actin-rich protrusions arise. Indeed, a recent study has shown a role of the shorter Cher isoform

501 (FLN90) that lacks actin-binding domains as a postsynaptic scaffold in *Drosophila* larval
502 neuromuscular junctions (Lee and Schwarz 2016); FLN90 is required for synaptic localization of
503 several key proteins, including type-A glutamate receptors and Ral GTPase (Lee and Schwarz
504 2016). Further studies will be needed to identify Jbug-interacting proteins and to reveal their
505 roles in helping Jbug organize higher-order actin structures.
506
507 **Jbug functions in epithelial morphogenesis**
508 Maternal knockdown of *jbug* using strong RNAi lines results in very few embryos, suggesting
509 Jbug functions in oogenesis. When a weaker RNAi line was used to knock down maternal *jbug*,
510 embryos with mostly normal morphology are generated. When *jbug* was knocked down both
511 maternally and zygotically using the same RNAi line, enhanced morphological defects were
512 observed (Figure 5), suggesting that both maternal and zygotic pools of *jbug* have roles in
513 epithelial morphogenesis. Dynamic localization of Jbug to the apical surface during
514 embryogenesis (Figures 4 and 5) further suggests roles for Jbug in remodeling the actin
515 cytoskeleton and contributing to the mechanical stability of the plasma membrane and the cell
516 cortex. Interestingly, in $jbug^{30}$ hypomorphic allele, where only Jbug-PC (the smallest isoform that
517 only contain short IG-FLMN repeats) and Jbug-PL (an intermediate isoform that contains actin-
518 binding domains and short IG-FLMN repeats) are intact, no overt defects are observed during
519 embryogenesis except for defects in denticle formation at later stages. As Jbug-PC is not
520 expressed in the embryo (Figure 1), these data indicate that Jbug-PL is sufficient for epithelial
521 morphogenesis during embryogenesis.

522 Several studies suggest roles for filamin A in tubular epithelial morphogenesis and diseases in
523 tubular organs. During branching of breast cells, the levels of filamin A expression and the
524 extent of the integrin-filamin interaction modulate collagen remodeling to optimize matrix
525 stiffness to support tubulogenesis (Gehler *et al.* 2009). Filamin A is also an important regulator
526 for Polycystin-2, a key molecule in autosomal polycystic kidney disease (Wang *et al.* 2015). Our
527 data also suggests a potential role for Jbug in apical domain reorganization in tubular epithelial
528 cells (Figure 6). Jbug shows strong apical enrichment in the embryonic trachea and the salivary
529 gland (Figure 5) and Jbug overexpression causes an expanded and irregular apical membrane
530 with dispersed Crb localization along the apical surface of salivary gland cells (Figure 6). These
531 data support the idea that appropriate levels of Jbug are important for apical organization during
532 tubular organ development. Loss of apical Jbug enrichment, however, does not cause overt
533 defects in tubular organ formation in *jbug* null or hypomorphic alleles, at least during

534 embryogenesis (Figure 5). In these alleles, abundant cytoplasmic Jbug signals still remain.
535 Overexpressed Jbug also mainly localizes to the cytoplasm in salivary gland cells (Figure 6).
536 These data suggest that apical enrichment may not be necessary for Jbug function in the
537 formation of tubular epithelia. Knockdown of *jbug* both maternally and zygotically (in the salivary
538 gland a few other tissues) results in severe morphological defects with an abnormal salivary
539 gland formation (Figure 5), indicating that tube formation will be quite abnormal in the complete
540 absence of *jbug* function.
541
542 **Potential roles for the smallest isoform Jbug-PC in the nucleus**
543 Jbug-PC only contains four IG-FLMN repeats and lacks actin-binding domains, suggesting that
544 the major mode of action of this smallest Jbug isoform is not cytoskeletal organization.
545 Compared to other Jbug isoforms that are continuously expressed throughout development,
546 Jbug-PC is abundant only during pupation (Figure 1), suggesting transient and specific roles for
547 Jbug-PC. Our study also shows that Jbug-PC localizes both to the nucleus and to the cytoplasm
548 when overexpressed in the embryonic salivary gland (Figure 6). Similar nuclear localization has
549 been observed in human Filamin A. Although full-length filamin A is predominantly cytoplasmic,
550 a C-terminal fragment of Filamin A colocalizes with androgen receptor to the nucleus to act as a
551 co-transcription factor (Loy *et al.* 2003). Therefore, a possible scenario is that Jbug-PC has a
552 role in transcriptional regulation. It will be interesting to test which developmental processes
553 require the function of Jbug-PC during pupation and to reveal its exact roles in those processes.
554
555 **Trans-splicing occurs in the *jbug* locus**
556 Trans-splicing, a gene regulatory mechanism that joins exons from two separate transcripts to
557 produce chimeric mRNA, has been detected in most eukaryotes (Horiuchi and Aigaki 2006;
558 Lasda and Blumenthal 2011). In *Drosophila*, trans-splicing has been demonstrated to be an
559 essential process for two genes, *longitudinals lacking* (*lola*) and *modifier of mdg4* (*mod(mdg4)*).
560 In the *lola* locus, the 5'-end of *lola* transcripts contain five exons that splice into 20 variants of 3'
561 exons to generate 20 protein isoforms (Ohsako *et al.* 2003). In the *mod(mdg4)* locus, two
562 mutant alleles of the gene, each located in one of the two homologous chromosomes, restore
563 the wild type function of the gene (Mongelard *et al.* 2002). This phenomenon is very similar to
564 the rescue that we have observed in $jbug^{30}$/*Exel6079* and $jbug^{133}$/*Exel6079* transheterozygotes
565 (Table 1). The presence of Jbug-PF/M/N isoforms in transheterozygous animals for *jbug*
566 hypomophs and *Exel6079* (Figure 2) further supports the idea that trans-splicing occurs, where
567 the 5' exons of *jbug-RF/M/N* transripts on $jbug^{30}$ or $jbug^{133}$ are spliced to 3' exons of *jbug*

568 transcripts on the *Exel6079* chromosome. Recent studies have revealed conserved sequences
569 in the *mod(mdg4)* intron that promote trans-splicing in this gene (Gao *et al.* 2015; Tikhonov *et al.*
570 2018). Identification of the sequences that promote trans-splicing in the *jbug* locus will help
571 better understand this surprising gene regulatory mechanism.
572
573

574 **Table 1. Complementation test**

575

	Number of Progeny	
	CyO	Non-CyO
jbug^{20}*/CyO* x *jbug*^{20}*/CyO*	>200	0
jbug^{20}*/CyO* x *Df(2R)59AB/CyO*	>200	0
jbug^{20}*/CyO* x *Df(2R)Exel6079/CyO*	>200	0
jbug^{30}*/CyO* x *jbug*^{20}*/CyO*	176	12*
jbug^{30} (F) x *jbug*^{20}*/CFL* (M)	144	50*
jbug^{30}*/CyO* x *Df(2R)59AB/CyO*	231	41*
jbug^{30}*/CyO* x *Df(2R)Exel6079/CyO*	98	91
jbug^{133}*/CyO* x *jbug*^{20}*/CyO*	141	62*
jbug^{133} (F) x *jbug*^{20}*/CFL* (M)	64	70*
Jbug^{133}*/CyO* x *Df(2R)59AB/CyO*	153	47*
jbug^{133}*/CyO* x *Df(2R)Exel6079/CyO*	140	100
* Transheterozygous flies show the same bristle defects as *jbug*^{30} or *jbug*^{133} homozygotes (See Figure 3 for phenotypes in homozygotes).		

576

577 **Figure legends**

578 **Figure 1. Different isoforms of *jbug* are expressed differentially throughout *Drosophila***
579 **development.** (A) Ten annotated splice forms of *jbug* are reported by FlyBase. Cyan bars
580 indicate three RNAi lines for *jbug* that were tested in this study. Two deficiency lines in the *jbug*
581 locus are also indicated. *Df(2R)59AB* deletes the region that spans the entire *jbug* locus.
582 *Df(2R)Exel6079* deletes only the N-terminal region of several *jbug* isoforms that have longer N-
583 termini, including *jbug-RF*, *RM*, *RN* and *RL*. (B) Six different Jbug protein isoforms are made
584 from the different annotated splice forms. Calponin homology domains (yellow pentagon) and
585 filamin-type immunoglobulin domains (green hexagon) are shown. Magenta bars in A and B
586 indicate the region used to generate Jbug antiserum. (C) Developmental RNA-Seq data by
587 Flybase (www.flybase.org; FB2020_04). Note that *jbug-RF*, *RM*, *RN* and *RL* are not expressed
588 until 18 hours of embryogenesis (red arrow). (D) Western blot using protein extracts from
589 embryos (0-2 and 2-16 hours AEL at 25°C), 1st, 2nd and 3rd instar larvae, pupae (2 days APF)
590 and male (M) and female (F) adults (2 days post-eclosion). A number of bands are detected.
591 Bands that correspond to the predicted molecular weights of several isoforms are marked with
592 dots and arrowheads with different colors. Arrowheads of the same colors are used to indicate
593 the major isoforms in B. Molecular mass (kDa) for protein size markers are shown on the left.
594

595 **Figure 1.**

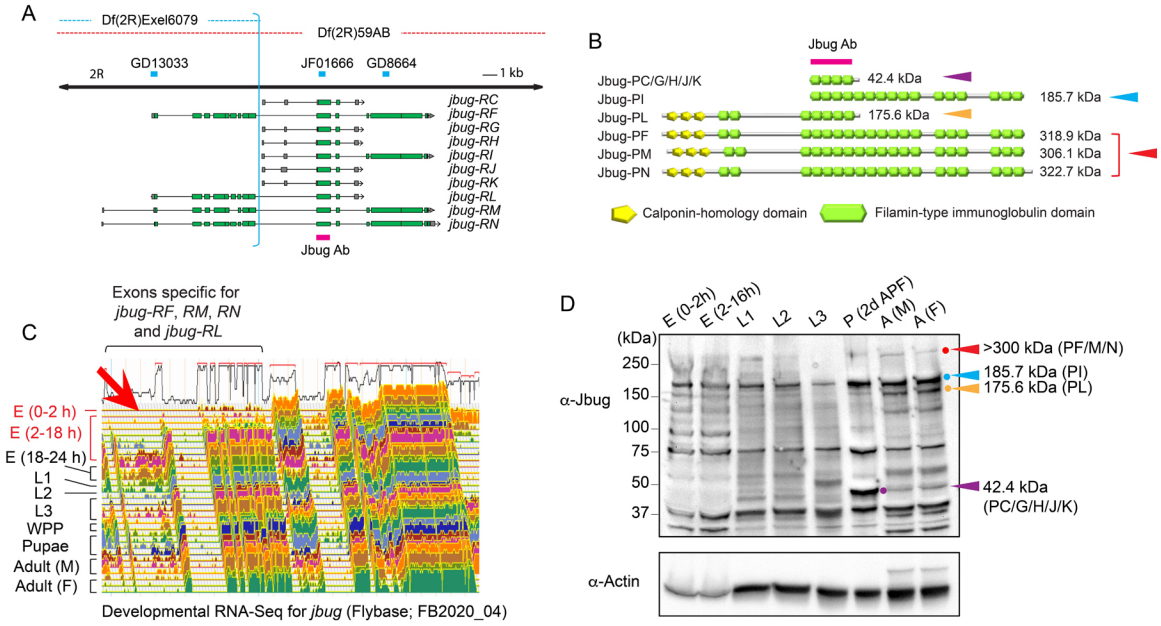

596

597

598 **Figure 2. Generation of null and hypomorphic alleles of *jbug*.** (A-D) Molecular alterations in
599 the null (*jbug*^{20}, A) and in two hypomorphic alleles (*jbug*^{30} and *jbug*^{133}, B-D). Blue and red boxes
600 represent homology arms that were used for homologous recombination. Magenta bar
601 represents a common exon for all isoforms that was used to generate an antibody against Jbug.
602 Two deficiency lines in the *jbug* locus are also indicated. *Df(2R)59AB* deletes the region that
603 spans the entire *jbug* locus. *Df(2R)Exel6079* deletes only the N-terminal region of several *jbug*
604 isoforms that have longer N-termini, including *jbug-RF*, *RM*, *RN* and *RL*. (A) *jbug*^{20} deletes
605 exons encoded by all *jbug* splice forms. (B) Hypomorphic alleles were generated by incomplete
606 homologous recombination, with a partial (*jbug*^{30}) or a complete (*jbug*^{133}) insertion of the donor
607 DNA into the *jbug* isoforms that have a longer C terminus (RF, RM, RN and RI). The insertion
608 occurs in the middle of the coding region or at the 3' UTR of those isoforms in *jbug*^{30} and *jbug*^{133},
609 respectively. (C and D) Detailed genomic structures of *jbug*^{30} and *jbug*^{133} alleles. (C) In *jbug*^{30},
610 one homology arm (red box) in the C-terminus region is recombined properly, but the rest of the
611 construct that contains the left homology arm (blue box) and the *mini-w*$^{+}$ fragment is inserted
612 into the *jbug* locus, disrupting several isoforms that have a longer C-terminus, including *jbug-RF*,
613 *RM, RN* and *RI*. (D) In *jbug*^{133}, the entire construct is inserted into the 3' UTR of *jbug-RF*, *RM*,
614 *RN* and *RI*. (E-H) Western blots using protein extracts from 2-16 hr embryos (E), 1st instar
615 larvae (F), pupae (2 days APF, G) and 2-day old female adults (H) show that different isoforms
616 are affected in each mutant. Bands that correspond to the predicted molecular weights of
617 several isoforms are marked with dots and arrowheads with different colors. Note that whereas
618 *jbug*^{20} embryos have most of the protein bands observed in wild type (E), almost all bands are
619 gone in 1st instar larvae (F), suggesting that protein from maternally provided *jbug* mRNA
620 persists during embryogenesis and is gone by the 1st instar larval stage. Asterisks in F, two
621 small bands that are still observed in *jbug*^{20} larvae, which could be a nonspecific cross-reactivity.
622 Distinct bands that correspond in size to annotated proteins are marked with dots and
623 arrowheads with different colors. Note that instead of an expected band for Jbug-PI (185.7 kDa,
624 blue arrow and dot), a shorter band (green arrow and dot; ~90 kDa) is observed in *jbug*^{30},
625 suggesting that a truncated protein for Jbug-PI is produced due to the insertion of the DNA
626 construct Note also that the large Jbug-PF/M/N (>300 kDa) band is also missing in the *jbug*^{30}
627 allele. *jbug*^{133} appears to show only a reduction in Jbug-PI (185.7 kDa) and the Jbug-PF/M/N
628 (>300 kDa bands). Thus, both *jbug*^{30} and *jbug*^{133} make wild type levels of Jbug-PL and Jbug-
629 PC/G/H/J/K, but *jbug*^{30} does not make PI or PF/M/N, and *jbug*^{133} makes reduced levels of PI
630 and PF/M/N. (I, J) Western blots using protein extracts from 2-16 hr embryos (I) and 1st instar
631 larvae (J). (I) In both *59AB* and *Exel6079* homozygous embryos, same protein bands are

632 detected as wild type. Bands that correspond to the predicted MWs of Jbug-PF/M/N, Jbug-PI
633 and Jbug-PL are marked with dots and arrowheads with different colors. Note that two faint but
634 distinct bands are visible for >300 KDa, suggesting that Jbug-PM (306.1 kDa) and the other two
635 bigger isoforms, Jbug-PF (318.9 kDa) and Jbug-PN (322.7 kDa), are separated in this gel. (J)
636 Whereas two clear bands for Jbug-PF/M/N (>300 kDa; red dots and arrowhead) are shown in
637 wild type, these bands are significantly decreased in *jbug*^{30} larvae. Jbug-PI (185.7 kDa; cyan
638 dots and arrowhead) is also clearly missing in *jbug*^{30}. In *jbug*^{30}*/Exel6079* transheterozygous
639 larvae, Jbug-PF/M/N, Jbug-PI and Jbug-PL bands are all detected, suggesting that transcripts
640 that initiate on the *jbug*^{30} chromosome can be transpliced with transcripts made from the
641 *Exel6079* chromosome.
642

Figure 2.

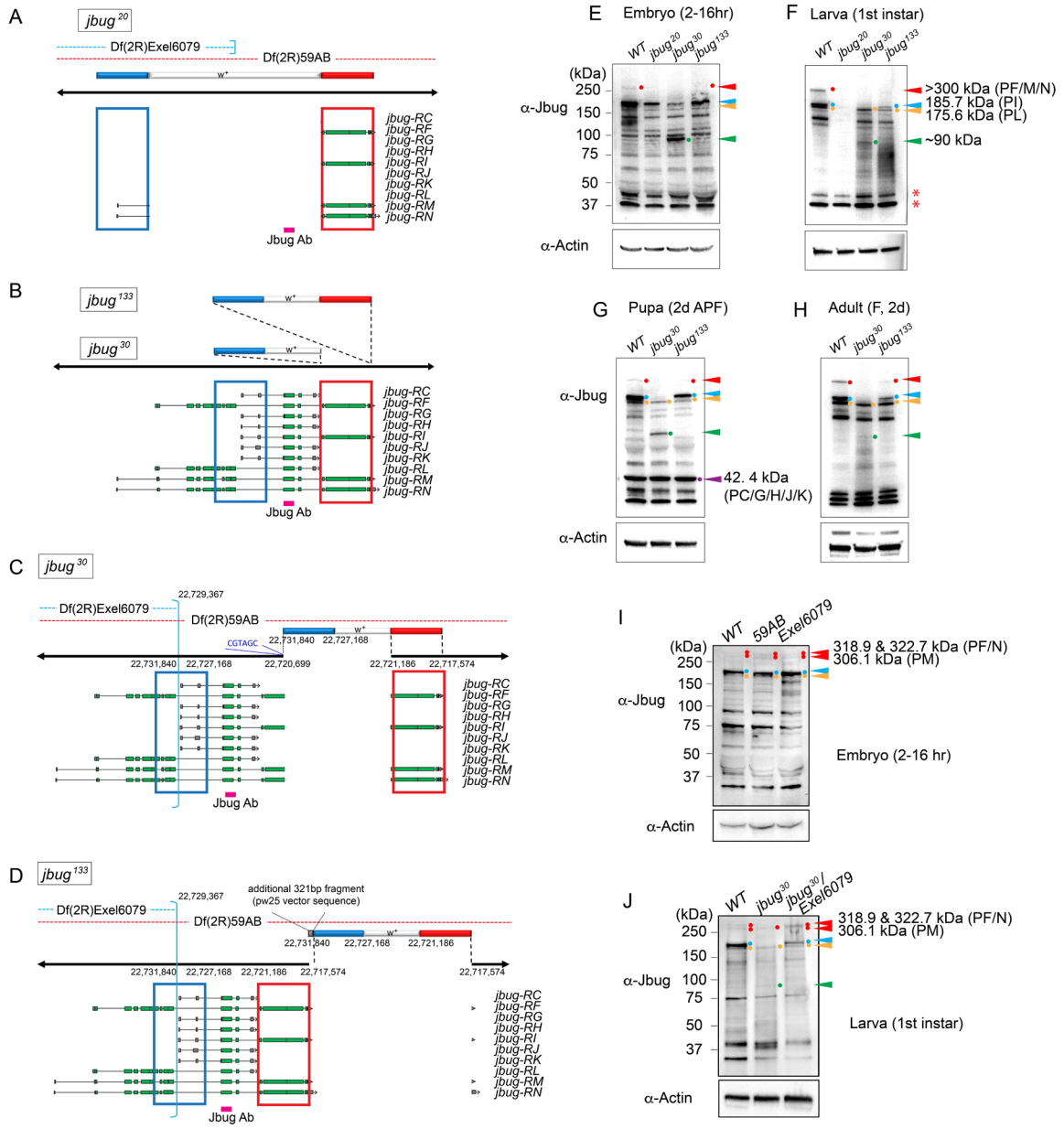
A
jbug 20
Df(2R)Exel6079
Df(2R)59AB
w+
jbug-RC
jbug-RF
jbug-RG
jbug-RH
jbug-RI
jbug-RJ
jbug-RK
jbug-RL
jbug-RM
jbug-RN
Jbug Ab
B
jbug 133
jbug 30
C
22,729,367
CGTAGC
22,731,840
22,727,168
22,720,699
22,721,186
22,717,574
D
additional 321bp fragment
(pw25 vector sequence)
E Embryo (2-16hr)
F Larva (1st instar)
WT
(kDa)
250
150
100
75
50
37
α-Jbug
α-Actin
>300 kDa (PF/M/N)
185.7 kDa (PI)
175.6 kDa (PL)
~90 kDa
G Pupa (2d APF)
H Adult (F, 2d)
42. 4 kDa
(PC/G/H/J/K)
I
59AB
Exel6079
318.9 & 322.7 kDa (PF/N)
306.1 kDa (PM)
Embryo (2-16 hr)
J
Larva (1st instar)

646 **Figure 3. *jbug*^{30} and *jbug*^{133} show bristle defects on the adult thorax, which are rescued**
647 **by expression of Jbug-RF.** (A) Compared to wild type, *jbug*^{30} and *jbug*^{133} adult flies show
648 distinct thoracic bristle defects, including short bristles with rough ends and bent bristles
649 (arrowheads). *jbug*^{133} flies have milder defects than *jbug*^{30}. (B) SEM images for bristles in wild
650 type and *jbug*^{30} male flies. Bristles in the red and yellow boxes on the flies are shown in higher
651 magnification in a-f. Compared to the nicely elongated and tapered wild-type bristle (a), bristles
652 in *jbug*^{30} mutants are short and distorted (c), bent (d), and rough-ended (e). Even when the
653 bristle looks relatively normal, it is often shorter than the wild type and slightly twisted (compare
654 b and f). (a'-f') Higher magnification of a-f is shown. (C, D) Whereas overexpression of Jbug-RC
655 using *69B-Gal4* or *da-Gal4* in an otherwise wild type animal does not cause overt defects in
656 thoracic bristles (C), overexpression of Jbug-RF causes short thick bristles (D; red arrowheads).
657 (E, F) Overexpression of Jbug-RC does not rescue the bristle defects in *jbug*^{30} (E; red
658 arrowheads). Jbug-RF expression almost completely rescues the bristle defects in *jbug*^{30} (F),
659 leaving only a couple of short bristles (blue arrowheads).
660

Figure 3.

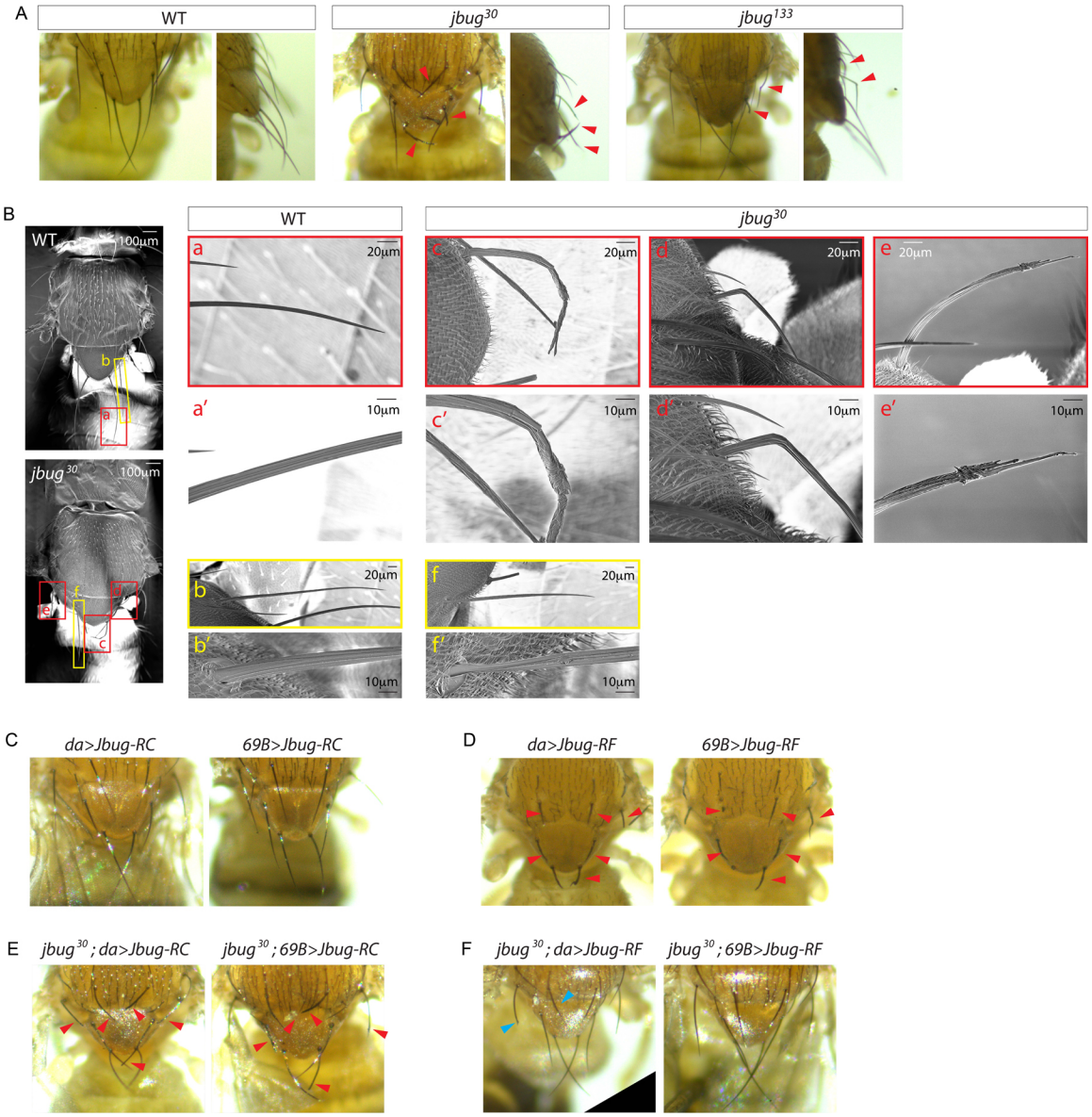
A
WT
jbug30
jbug133
B
WT
100µm
jbug30
100µm
WT
jbug30
a
20µm
c
20µm
d
20µm
e
20µm
a′
10µm
c′
10µm
d′
10µm
e′
10µm
b
20µm
f
20µm
b′
10µm
f′
10µm
C
da>Jbug-RC
69B>Jbug-RC
D
da>Jbug-RF
69B>Jbug-RF
E
jbug30; da>Jbug-RC
jbug30; 69B>Jbug-RC
F
jbug30; da>Jbug-RF
jbug30; 69B>Jbug-RF

664 **Figure 4. Analysis of Jbug protein localization in the embryonic epidermis in different**
665 ***jbug* alleles.** (A) Confocal images for early embryos stained for Jbug (green) and phalloidin
666 (magenta). Jbug localizes as small apical punctate structures. (B-K) Confocal images for
667 epidermis in stage 13 (B, D, F, H, J) and stage 15 (C, E, G, I, K) embryos stained for Jbug
668 (green) and E-Cad (magenta). (B, C) In wild type, whereas high Jbug signals are observed both
669 on the apical surface (arrowheads) and at adherens junctions (arrows) at stage 13 (B), Jbug
670 mostly localizes more uniformly across the apical surface (arrowheads) at stage 15 (C). (D, E)
671 In *jbug*^{20} mutants, junctional Jbug signals are absent and signals on the apical surface are weak
672 (arrows in D). (F, G) In *jbug*^{30} mutants, overall Jbug signals are very weak and diffused
673 throughout the stages. (H, I) In *jbug*^{133} embryos, signals at both the apical surface (arrowheads)
674 and junctions (arrows) are present but are slightly weaker than wild type. (J, K) Jbug-RF
675 overexpression in ectodermal cells driven by *69B-Gal4* in the *jbug*^{30} mutant background (J)
676 results in upregulation of Jbug signals in the entire apical domain with junctional enrichment at
677 stage 13 (arrows). Overexpression of Jbug-RF in all cells by *da-Gal4* in the *jbug*^{30} mutant
678 background (K) causes upregulation of Jbug signals in the apical domain at stage 15
679 (arrowheads).
680

681 **Figure 4.**

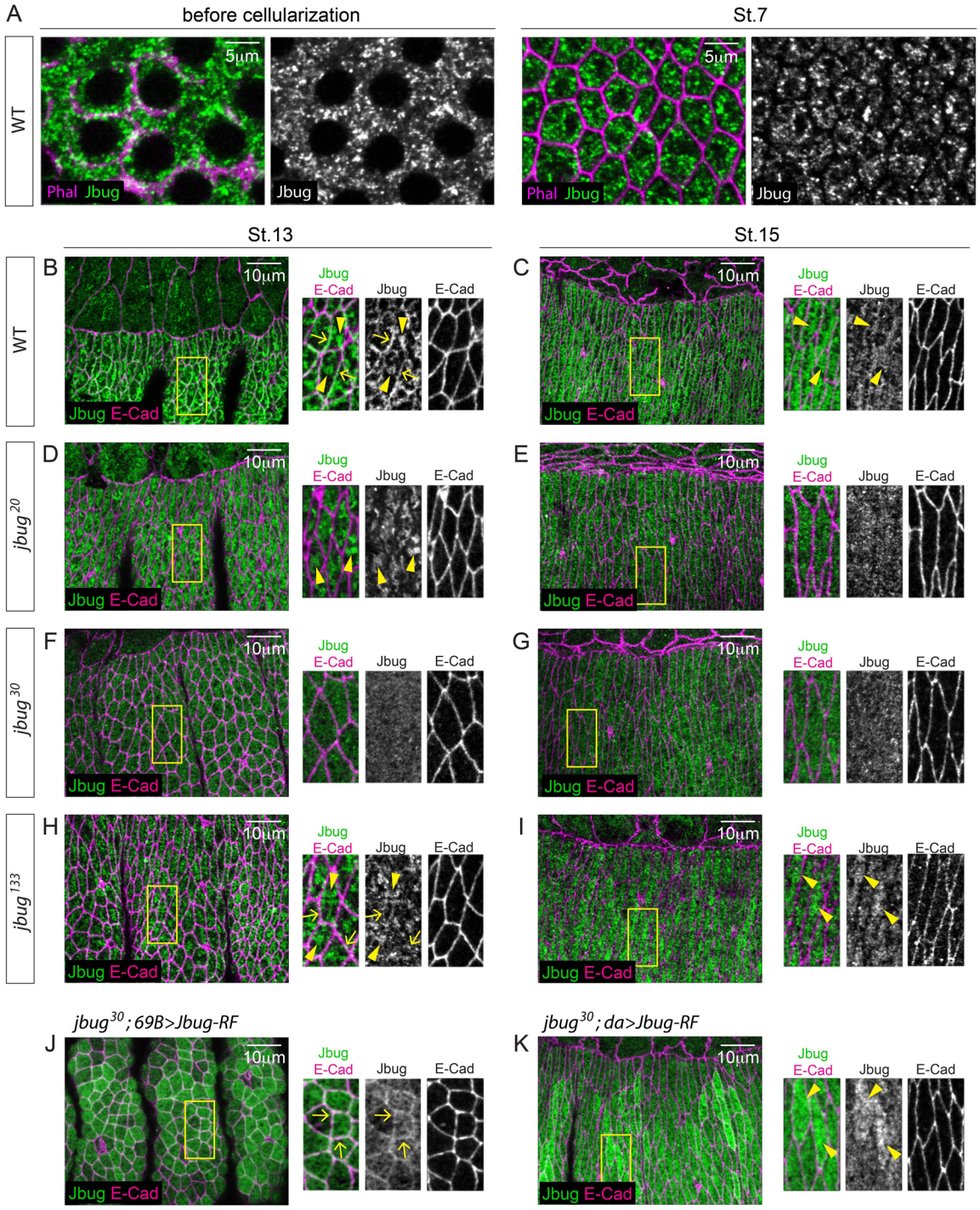

682

683

684 **Figure 5. Jbug protein is apically enriched in the embryonic trachea and the salivary**
685 **gland and this enrichment is absent in *jbug*^{20} and *jbug*^{30} mutants.** (A-D) Confocal images of
686 stage 14 embryonic trachea stained for Jbug (green) and E-Cad (magenta). (A) In wild type,
687 weak Jbug signals are observed in all tracheal cells, with enrichment in the apical domain
688 (arrowheads). (B) In *jbug*^{20} embryos, Jbug signals in the trachea are mostly absent (arrows). (C)
689 In *jbug*^{30} mutant embryos, Jbug signals are diffused in the cytoplasm in tracheal cells (asterisks),
690 with no apical enrichment (arrows; compare to E-Cad signals (arrowheads) in the apical
691 domain). (D) In *jbug*^{133}, apical enrichment of Jbug is still present (arrowheads). (E-H) Stage 14
692 salivary glands stained for Jbug (green) and E-Cad (magenta). (E) Similar to tracheal signals,
693 Jbug is enriched in the apical domain of wild type salivary gland cells (arrowheads) with weak
694 signals in the cytoplasm. (F) In *jbug*^{20}, overall Jbug signals are significantly decreased in the
695 salivary gland and apical enrichment is mostly gone (arrow; compare to E-Cad signals
696 (arrowhead) in the apical domain). (G) In *jbug*^{30}, Jbug is not apically enriched in the salivary
697 gland (arrow; compare to E-Cad signals (arrowhead) in the apical domain) but diffused in the
698 cytoplasm. (H) In *jbug*^{133}, apical enrichment of Jbug is still present (arrowheads). (I, J)
699 Reconstructed confocal images of stage 11 embryos stained for Crb (green, an apical marker)
700 and CrebA (magenta, a salivary gland nuclear marker). Ventrolateral view. Anterior is to the left.
701 Compared to wild type (I), maternal and zygotic knockdown of *jbug* (J) results in a disrupted
702 embryonic morphology. Salivary glands (yellow boxes) are shown in a higher magnification. 3D
703 reconstruction (top) and a single confocal section of the apical surface (bottom) are shown.
704 Compared to a thin salivary gland lumen (arrow in I) and a small invagination pit (asterisks in I),
705 maternal and zygotic knockdown of *jbug* results in a wider lumen (arrow in J) and an eloganted
706 invagination pit (asterisks in J).
707

708 **Figure 5.**

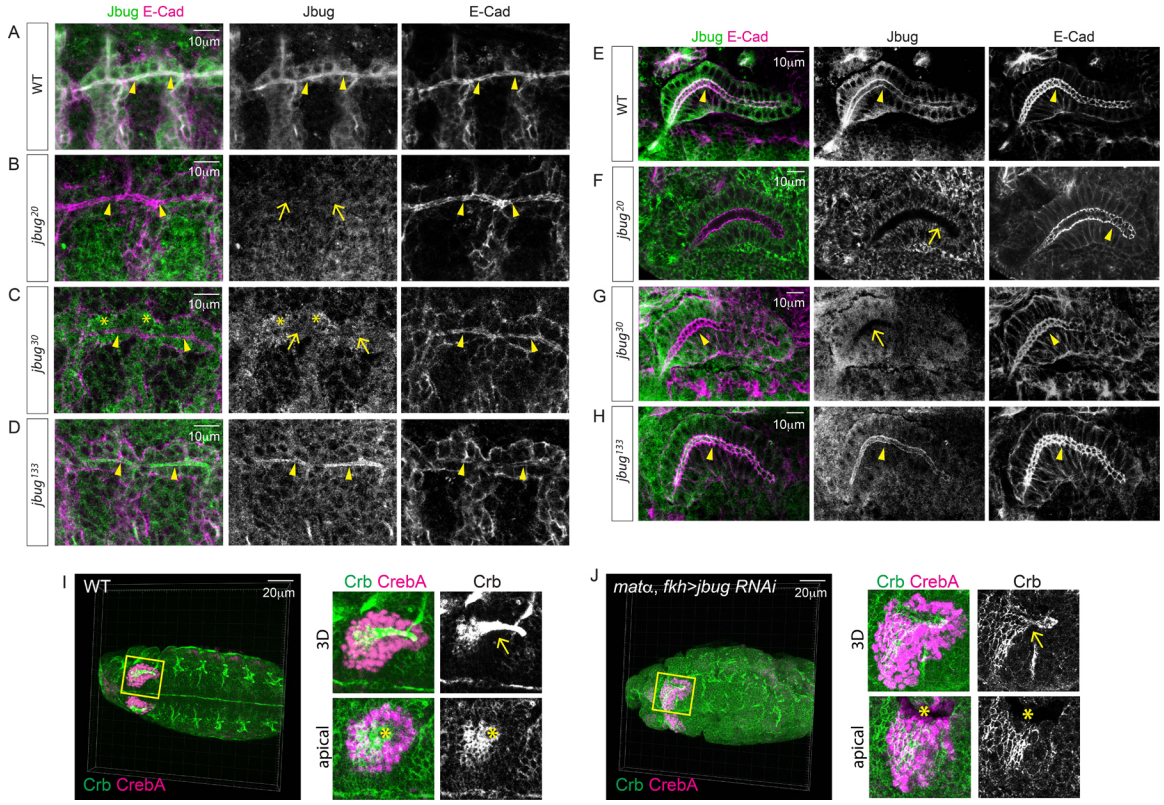

709

710

711 **Figure 6. Jbug overexpression causes mislocalization of Crb along the apical surface**
712 **and an expanded and irregular apical domain in the embryonic salivary gland.** (A-D) stage
713 16 salivary glands stained for Crb (green), Jbug (magenta), GFP (magenta in C) and salivary
714 gland nuclear markers CrebA (A, B, C, E and F) and Sage (D). Salivary glands overexpressing
715 Tmem-GFP (control, A), Jbug-RC (B), Jbug-RC-GFP (C), Jbug-RL (D) and Jbug-RF (E, F) are
716 shown. Note that Jbug mainly localizes to the cytoplasm and only shows weak apical signals in
717 stage 16 salivary glands (red arrow in A; compare to Figure 5E). Jbug-RC (B) and Jbug-RC-
718 GFP (C) localize both to salivary gland nuclei and to the cytoplasm when overexpressed. Jbug
719 overexpression causes an expanded and irregular salivary gland lumen (B-F). Irregular salivary
720 gland lumen is worsened when stronger UAS lines are used (compare B and C; also compare E
721 and F). Compared to subapical Crb signals along AJs in control salivary gland cells (inset in A;
722 yellow arrows), Crb signals are dispersed along the entire apical domain in Jbug-overexpressing
723 salivary glands (insets in B-F).
724

Figure 6.

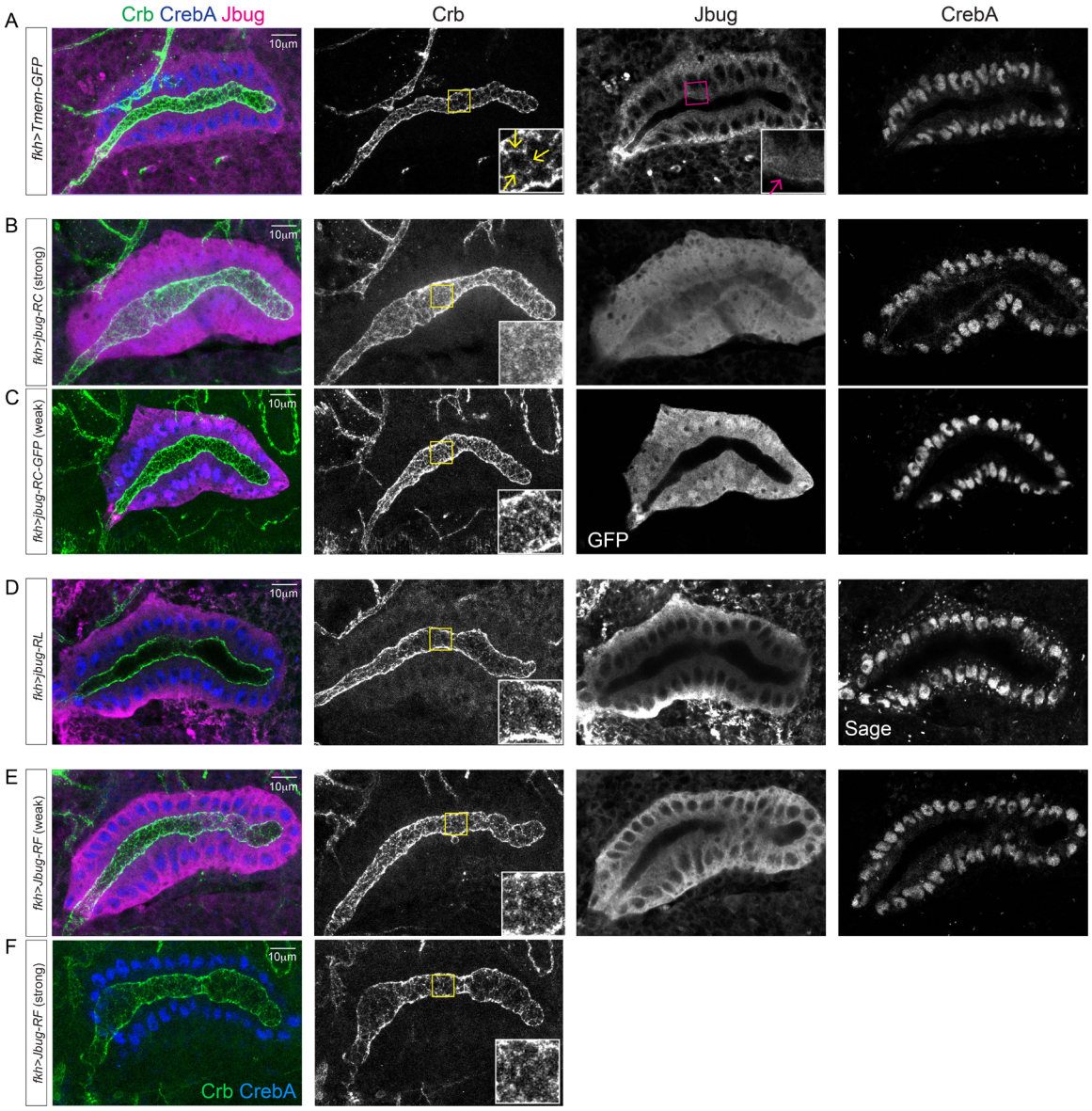
A
Crb CrebA Jbug
Crb
Jbug
CrebA
fkh> Tmem-GFP
10µm
B
fkh>jbug-RC (strong)
C
fkh>jbug-RC-GFP (weak)
GFP
D
fkh>jbug-RL
Sage
E
fkh>Jbug-RF (weak)
F
fkh>Jbug-RF (strong)
Crb CrebA

728 **Figure 7. Jbug protein is upregulated in the anterior part of each segment just prior to the**
729 **formation of actin-rich denticles in the same region.** (A-D) Epidermis in stages 13 (A), 14
730 (B), 15 (C) and 16 (D) embryos stained for phalloidin (red), Jbug (green) and E-Cad (magenta).
731 (A) At stage 13, Jbug is mostly uniform across epidermis. (B) At stage 14, actin begins to be
732 upregulated in the anterior side of each segment. Jbug also shows accumulation in the apical
733 domain of epidermal cells in the anterior side of the segment. (C-D) At stages 15 (C) and 16 (D),
734 actin-rich denticles form in the anterior side of each segment. Jbug still shows higher levels in
735 those regions. A and P represent the anterior and the posterior side, respectively. Yellow dotted
736 lines, ventral midline.
737

Figure 7.

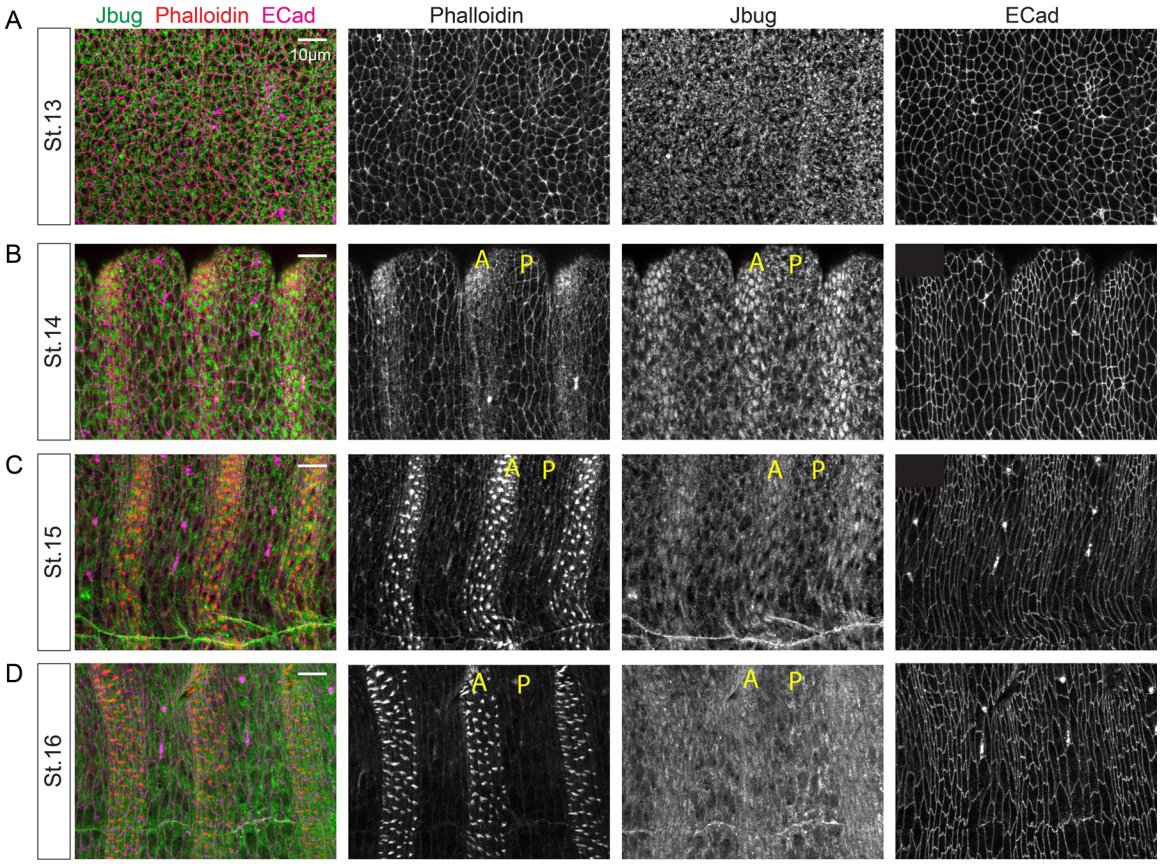
A
Jbug Phalloidin ECad
Phalloidin
Jbug
ECad
St.13
10μm
B
St.14
A P
C
St.15
D
St.16

741 **Figure 8. Jbug regulates the formation of denticle precursors in the ventral epidermis of**
742 **the embryo.** (A-G) Stage 16 embryos stained for E-Cad (magenta; cell boundaries) and
743 phalloidin (green; denticles). Ventral epidermis in wild type (A), *jbug*^{20} (B) *jbug*^{30} (C), *jbug*^{30} ;*da-*
744 *Gal4>Jbug-RF* (D), *da-Gal4>UAS-Jbug-RF* (E), *da-Gal4>jbug RNAi* (*GD13033*) (F) and *matα-*
745 *Gal4>jbug RNAi* (*JF01166*) (G) is shown. (A) Epidermal cells at the denticle belt in the
746 abdominal segment 5 (yellow box) are shown at higher magnification. Dotted yellow lines,
747 ventral midline. (B-G) Epidermal cells of the same region as in A are shown. For all the embryos,
748 anterior is to the left. (B, G) *jbug*^{20} mutants and embryos maternally knocked down *jbug* show
749 mild defects in the embryo morphology, such as wavy epidermis (red arrowheads in B and G;
750 cells are out of focus). Occasionally, cells either fail to form denticles (white arrowhead in G) or
751 form very short denticles (orange arrowheads in B and G). (H) A cartoon for quantification of the
752 denticle numbers. Four cells that are closest to the ventral midline were chosen in each of the
753 six columns of cells in denticle belts in abdominal segments 4, 5 and 6 (column 1, most anterior).
754 (I) Percentage of cells that have different numbers of denticles. (J) Quantification of the average
755 number of denticles per cell in each column of the belt. Student's t-test with Welch's correction
756 is used for statistics calculation. (K, L) Reconstructed 3D images for stage 16 wild type (K) and
757 *matα-Gal4>jbug RNAi* (L) embryos stained for Crb (green; apical membrane) and CrebA
758 (magenta; salivary gland nuclear marker). Maternal knockdown of *jbug* does not cause overt
759 morphological defects in the embryo, except for uneven epidermis (yellow arrows in L).
760

Figure 8.

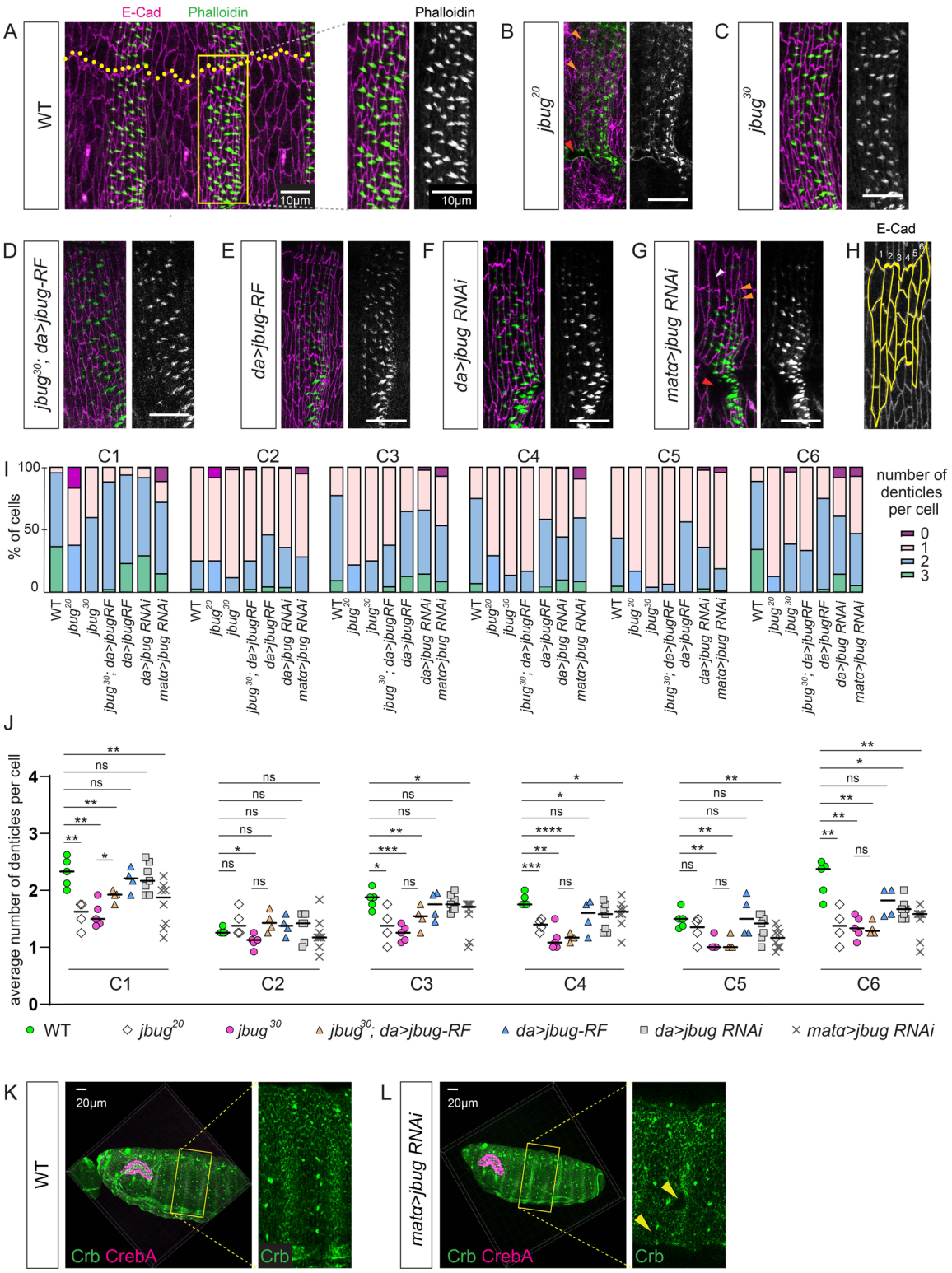
A
E-Cad
Phalloidin
Phalloidin
WT
10µm
10µm
B
jbug20
C
jbug30
D
jbug30; da>jbug-RF
E
da>jbug-RF
F
da>jbug RNAi
G
matα>jbug RNAi
H
E-Cad
I
C1
C2
C3
C4
C5
C6
% of cells
number of denticles per cell
0
1
2
3
WT
jbug20
jbug30
jbug30; da>jbugRF
da>jbugRF
da>jbug RNAi
matα>jbug RNAi
J
average number of denticles per cell
WT
jbug20
jbug30
jbug30; da>jbug-RF
da>jbug-RF
da>jbug RNAi
matα>jbug RNAi
K
WT
20µm
Crb CrebA
Crb
L
matα>jbug RNAi
20µm
Crb CrebA
Crb

763 **Supplemental Figure 1. Reverse transriptase-PCR (RT-PCR) reveals a loss of *jbug* mRNA**
764 **in *jbug*^{20} null mutants.** (A) Genomic structures for the jbug locus. Blue and red arrows
765 represent primers used for RT-PCR. (B and C) RT-PCR using cDNAs made from wild type (OR)
766 and *jbug*^{20} homozygous embryos. Whereas RT-PCR using wild type cDNA produces a PCR
767 product of expected sizes (left lanes in B and C), no bands are detected in *jbug*^{20} (right lanes in
768 B and C).
769

770 **Supplemental Figure 1.**

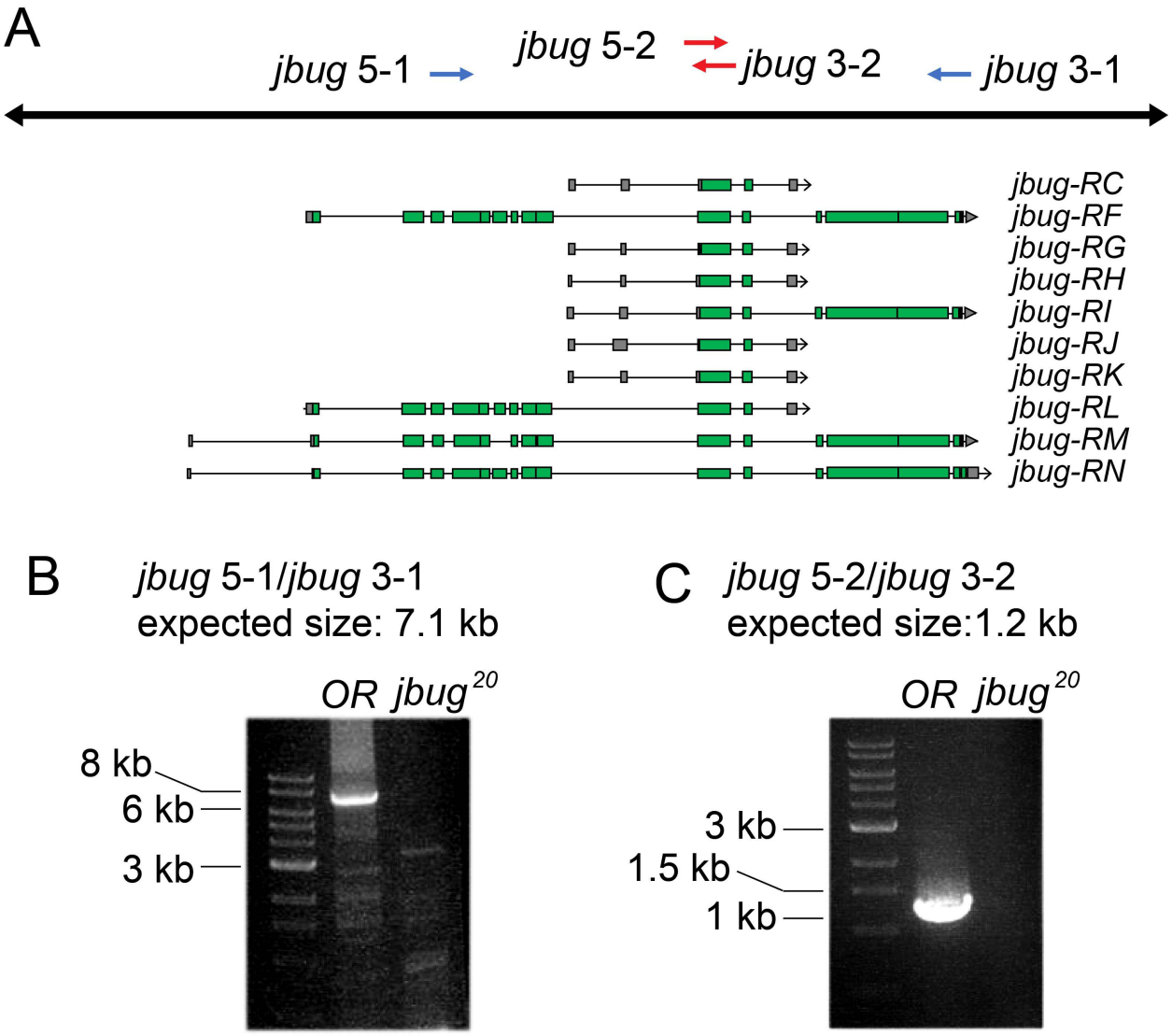

771

772

773 **Supplemental Figure 2. Mutations in *jbug* cause mild planar cell polarity defects in adult**
774 **wing hair orientation.** (A-C) Compared to relatively distal orientation of wing hairs in the wild
775 type wing (A), wings in *jbug*^{30} (B) and *jbug*^{133} (C) mutants show mild swirling patterns of wing
776 hairs. White boxed regions are shown in higher magnification in the bottom. (D, E) Wild type (D)
777 and *jbug*^{30} mutant (E) pupal wings (32 hours APF) stained for phalloidin. Prehair formation is
778 delayed in the pupal wing in in *jbug*^{30}. (F, G) Adult ommatidia of wild type (F) and *jbug*^{30} (G)
779 near the dorsal/ventral boundary, the equator. Schematic drawings are shown in the panels
780 below the actual images. Green and magenta shapes indicate the orientation of ommatidia that
781 is normally found in the dorsal and ventral hemisphere of the eye, respectively. *jbug*^{30} flies do
782 not show planar cell polarity defects in the orientation of ommatidia.
783

784 **Supplemental Figure 2.**

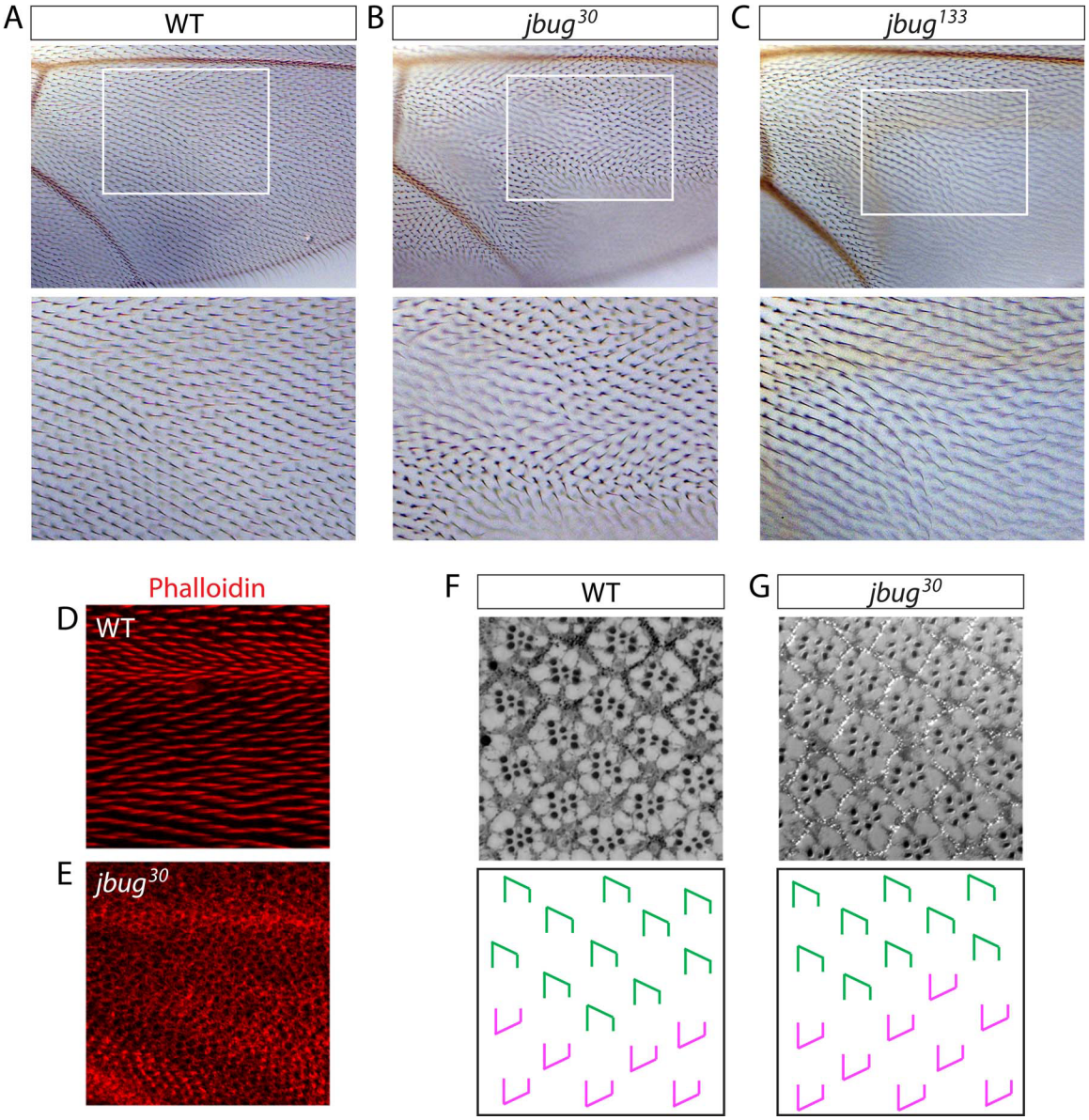

785
786

Acknowledgments

We thank the members of the Chung and the Andrew laboratories for comments and suggestions. We thank M. Mlodzik and the Bloomington stock center for fly stocks and the Developmental Studies Hybridoma Bank for antibodies. We thank Flybase for the gene information. This work is supported by start-up fund from Louisiana State University to S.C. and NIH RO1 DE013899 to D.A.

References

Adler P. N., 2012 The frizzled/stan pathway and planar cell polarity in the Drosophila wing. Curr. Top. Dev. Biol. 101: 1–31. https://doi.org/10.1016/b978-0-12-394592-1.00001-6

Bedolla R. G., Y. Wang, A. Asuncion, K. Chamie, S. Siddiqui, *et al.*, 2009 Nuclear versus cytoplasmic localization of filamin a in prostate cancer: Immunohistochemical correlation with metastases. Clin. Cancer Res. 15: 788–796. https://doi.org/10.1158/1078-0432.CCR-08-1402

Bejsovec A., 2013 Wingless/Wnt signaling in Drosophila: The pattern and the pathway. Mol. Reprod. Dev. 80: 882–894. https://doi.org/10.1002/mrd.22228

Browne K. A., R. W. Johnstone, D. A. Jans, and J. A. Trapani, 2000 Filamin (280-kDa actin-binding protein) is a caspase substrate and is also cleaved directly by the cytotoxic T lymphocyte protease granzyme B during apoptosis. J. Biol. Chem. 275: 39262–39266. https://doi.org/10.1074/jbc.C000622200

Chung S. Y., C. Chavez, and D. J. Andrew, 2011 Trachealess (Trh) regulates all tracheal genes during Drosophila embryogenesis. Dev. Biol. 360: 160–172. https://doi.org/10.1016/j.ydbio.2011.09.014

Chung S., and D. J. Andrew, 2014 Cadherin 99C regulates apical expansion and cell rearrangement during epithelial tube elongation. Development 141: 1950–60. https://doi.org/10.1242/dev.104166

Dilks S. A., and S. DiNardo, 2010 Non-cell-autonomous control of denticle diversity in the Drosophila embryo. Development 137: 1395–1404. https://doi.org/10.1242/dev.045450

Flier A. Van der, and A. Sonnenberg, 2001 Structural and functional aspects of filamins. Biochim. Biophys. Acta - Mol. Cell Res. 1538: 99–117. https://doi.org/10.1016/S0167-4889(01)00072-6

Fox R. M., A. Vaishnavi, R. Maruyama, and D. J. Andrew, 2013 Organ-specific gene expression: The bHLH protein Sage provides tissue specificity to Drosophila FoxA. Dev. 140: 2160–2171. https://doi.org/10.1242/dev.092924

Gao J. L., Y. J. Fan, X. Y. Wang, Y. Zhang, J. Pu, *et al.*, 2015 A conserved intronic U1 snRNP-binding sequence promotes trans-splicing in Drosophila. Genes Dev. 29: 760–771. https://doi.org/10.1101/gad.258863.115

Gay O., B. Gilquin, F. Nakamura, Z. A. Jenkins, R. McCartney, *et al.*, 2011 RefilinB (FAM101B) targets FilaminA to organize perinuclear actin networks and regulates nuclear shape. Proc. Natl. Acad. Sci. U. S. A. 108: 11464–11469. https://doi.org/10.1073/pnas.1104211108

Gehler S., M. Baldassarre, Y. Lad, J. L. Leight, M. A. Wozniak, *et al.*, 2009 Filamin A–ᴺᴸ1

828 Integrin Complex Tunes Epithelial Cell Response to Matrix Tension. Mol. Biol. Cell 20:
829 3224–3238. https://doi.org/10.1091/mbc.E08
830 Gong W. J., and K. G. Golic, 2003 Ends-out, or replacement, gene targeting in Drosophila. Proc.
831 Natl. Acad. Sci. U. S. A. 100: 2556–2561. https://doi.org/10.1073/pnas.0535280100
832 Gorlin J. B., R. Yamin, S. Egan, M. Stewart, T. P. Stossel, *et al.*, 1990 Human endothelial actin-
833 binding protein (ABP-280, nonmuscle filamin): A molecular leaf spring. J. Cell Biol. 111:
834 1089–1105. https://doi.org/10.1083/jcb.111.3.1089
835 Häcker U., and N. Perrimon, 1998 DRhoGEF2 encodes a member of the Dbl family of
836 oncogenes and controls cell shape changes during gastrulation in Drosophila. Genes Dev.
837 12: 274–284. https://doi.org/10.1101/gad.12.2.274
838 Henderson K. D., and D. J. Andrew, 2000 Regulation and function of Scr, exd, and hth in the
839 Drosophila salivary gland. Dev. Biol. 217: 362–374. https://doi.org/10.1006/dbio.1999.9560
840 Horiuchi T., and T. Aigaki, 2006 Alternative trans-splicing: a novel mode of pre-mRNA
841 processing. Biol. Cell 98: 135–140. https://doi.org/10.1042/bc20050002
842 Huelsmann S., N. Rintanen, R. Sethi, N. H. Brown, and J. Ylänne, 2016 Evidence for the
843 mechanosensor function of filamin in tissue development. Sci. Rep. 6: 2–9.
844 https://doi.org/10.1038/srep32798
845 Krueger D., T. Quinkler, S. A. Mortensen, C. Sachse, and S. de Renzis, 2019 Cross-linker–
846 mediated regulation of actin network organization controls tissue morphogenesis. J. Cell
847 Biol. 218: 2743–2761. https://doi.org/10.1083/JCB.201811127
848 Külshammer E., and M. Uhlirova, 2013 The actin cross-linker filamin/cheerio mediates tumor
849 malignancy downstream of JNK signaling. J. Cell Sci. 126: 927–938.
850 https://doi.org/10.1242/jcs.114462
851 Lasda E. L., and T. Blumenthal, 2011 Trans-splicing. Wiley Interdiscip. Rev. RNA 2: 417–434.
852 https://doi.org/10.1002/wrna.71
853 Lee G. Y., and T. L. Schwarz, 2016 Filamin, a synaptic organizer in Drosophila, determines
854 glutamate receptor composition and membrane growth. Elife 5: 1–29.
855 https://doi.org/10.7554/eLife.19991
856 Li M., M. Serr, K. Edwards, S. Ludmann, D. Yamamoto, *et al.*, 1999 during Drosophila
857 Oogenesis. Cell 146: 1061–1073.
858 Loy C. J., K. S. Sim, and E. L. Yong, 2003 Filamin-A fragment localizes to the nucleus to
859 regulate androgen receptor and coactivator functions. Proc. Natl. Acad. Sci. U. S. A. 100:
860 4562–4567. https://doi.org/10.1073/pnas.0736237100
861 Manieu C., G. H. Olivares, F. Vega-Macaya, M. Valdivia, and P. Olguín, 2018 Jitterbug/Filamin

862 and Myosin-II form a complex in tendon cells required to maintain epithelial shape and
863 polarity during musculoskeletal system development. Mech. Dev. 154: 309–314.
864 https://doi.org/10.1016/j.mod.2018.09.002
865 Mongelard F., M. Labrador, E. M. Baxter, T. I. Gerasimova, and V. G. Corces, 2002 Trans-
866 splicing as a novel mechanism to explain interallelic complementation in Drosophila.
867 Genetics 160: 1481–1487.
868 Nakamura F., T. P. Stossel, and J. H. Hartwig, 2011 The filamins: Organizers of cell structure
869 and function. Cell Adh. Migr. 5: 160–169. https://doi.org/10.4161/cam.5.2.14401
870 Ohsako T., T. Horiuchi, T. Matsuo, S. Komaya, and T. Aigaki, 2003 Drosophila lola encodes a
871 family of BTB-transcription regulators with highly variable C-terminal domains containing
872 zinc finger motifs. Gene 311: 59–69. https://doi.org/10.1016/S0378-1119(03)00554-7
873 Ohta Y., and J. H. Hartwig, 1996 Phosphorylation of actin-binding protein 280 by growth factors
874 is mediated by p90 ribosomal protein S6 kinase. J. Biol. Chem. 271: 11858–11864.
875 https://doi.org/10.1074/jbc.271.20.11858
876 Olguín P., A. Glavic, and M. Mlodzik, 2011 Intertissue mechanical stress affects Frizzled-
877 mediated planar cell polarity in the Drosophila notum epidermis. Curr. Biol. 21: 236–42.
878 https://doi.org/10.1016/j.cub.2011.01.001
879 Oliva C., C. Molina-Fernandez, M. Maureira, N. Candia, E. L??pez, *et al.*, 2015 Hindsight
880 regulates photoreceptor axon targeting through transcriptional control of jitterbug/Filamin
881 and multiple genes involved in axon guidance in Drosophila. Dev. Neurobiol. 75: 1018–
882 1032. https://doi.org/10.1002/dneu.22271
883 Razinia Z., T. Mäkelä, J. Ylänne, and D. a Calderwood, 2012 Filamins in mechanosensing and
884 signaling. Annu. Rev. Biophys. 41: 227–46. https://doi.org/10.1146/annurev-biophys-
885 050511-102252
886 Rorth Pe., 1996 A modular misexpression screen in Drosophila detecting tissue-specific
887 phenotypes. Proc. Natl. Acad. Sci. 93: 12418–12422.
888 Sasaki E., A. T. Byrne, E. Phelan, D. W. Cox, and W. Reardon, 2019 A review of filamin A
889 mutations and associated interstitial lung disease. Eur. J. Pediatr. 178: 121–129.
890 https://doi.org/10.1007/s00431-018-3301-0
891 Savoy R. M., and P. M. Ghosh, 2013 The dual role of filamin A in cancer: Can't live with (too
892 much of) it, can't live without it. Endocr. Relat. Cancer 20: 341–356.
893 https://doi.org/10.1530/ERC-13-0364
894 Shao Q. Q., T. P. Zhang, W. J. Zhao, Z. W. Liu, L. You, *et al.*, 2016 Filamin A: Insights into its
895 Exact Role in Cancers. Pathol. Oncol. Res. 22: 245–252. https://doi.org/10.1007/s12253-

896 015-9980-1
897 Sokol N. S., and L. Cooley, 1999 Drosophila Filamin encoded by the cheerio locus is a
898 component of ovarian ring canals. Curr. Biol. 9: 1221–1230. https://doi.org/10.1016/S0960-
899 9822(99)80502-8
900 Sokol N. S., and L. Cooley, 2003 Drosophila filamin is required for follicle cell motility during
901 oogenesis. Dev. Biol. 260: 260–272. https://doi.org/10.1016/S0012-1606(03)00248-3
902 Song J., and M. A. Tanouye, 2006 Seizure suppression by shakB2, a gap junction mutation in
903 Drosophila. J. Neurophysiol. 95: 627–635. https://doi.org/10.1152/jn.01059.2004
904 Tepass U., 1996 Crumbs, a component of the apical membrane, is required for zonula adherens
905 formation in primary epithelia of Drosophila. Dev. Biol. 177: 217–225.
906 https://doi.org/10.1006/dbio.1996.0157
907 Thurmond J., J. L. Goodman, V. B. Strelets, H. Attrill, L. S. Gramates, *et al.*, 2019 FlyBase 2.0:
908 The next generation. Nucleic Acids Res. 47: D759–D765.
909 https://doi.org/10.1093/nar/gky1003
910 Tikhonov M., M. Utkina, O. Maksimenko, and P. Georgiev, 2018 Conserved sequences in the
911 Drosophila mod(mdg4) intron promote poly(A)-independent transcription termination and
912 trans-splicing. Nucleic Acids Res. 46: 10608–10618. https://doi.org/10.1093/nar/gky716
913 Tirupula K. C., S. S. Ithychanda, M. L. Mohan, S. V. Naga Prasad, J. Qin, *et al.*, 2015 G protein-
914 coupled receptors directly bind filamin A with high affinity and promote filamin
915 phosphorylation. Biochemistry 54: 6673–6683.
916 https://doi.org/10.1021/acs.biochem.5b00975
917 Wang Y., J. I. Kreisberg, R. G. Bedolla, M. Mikhailova, R. W. Devere White, *et al.*, 2007 A 90
918 kDa fragment of filamin A promotes Casodex-induced growth inhibition in Casodex-
919 resistant androgen receptor positive C4-2 prostate cancer cells. Oncogene 26: 6061–6070.
920 https://doi.org/10.1038/sj.onc.1210435
921 Wang Q., W. Zheng, Z. Wang, J. W. Yang, S. Hussein, *et al.*, 2015 Filamin-A increases the
922 stability and plasma membrane expression of polycystin-2. PLoS One 10: 1–19.
923 https://doi.org/10.1371/journal.pone.0123018
924 Wodarz A., U. Hinz, M. Engelbert, and E. Knust, 1995 Expression of crumbs confers apical
925 character on plasma membrane domains of ectodermal epithelia of drosophila. Cell 82:
926 67–76. https://doi.org/10.1016/0092-8674(95)90053-5
927 Yue J., S. Huhn, and Z. Shen, 2013 Complex roles of filamin-A mediated cytoskeleton network
928 in cancer progression. Cell Biosci. 3: 1. https://doi.org/10.1186/2045-3701-3-7
929